Check for updates

JGR Earth Surface

RESEARCH ARTICLE
10.1029/2021JF006437

Near-Bed Structure of Sediment Gravity Flows Measured by Motion-Sensing "Boulder-Like" Benthic Event Detectors (BEDs) in Monterey Canyon

R. Gwiazda[1], C. K. Paull[1], B. Kieft[1], D. Klimov[1], R. Herlien[1], E. Lundsten[1], M. McCann[1], Matthieu J. Cartigny[2], A. Hamilton[1], J. Xu[3], Katherine L. Maier[4,5], D. R. Parsons[6], and Peter J. Talling[7]

[1]Monterey Bay Aquarium Research Institute, Moss Landing, CA, USA, [2]Geography Department, Durham University, Durham, UK, [3]Department of Ocean Science and Engineering, Southern University of Science and Technology, Shenzhen, Guangdong, China, [4]U.S. Geological Survey, Pacific Coastal and Marine Science Center, Santa Cruz, CA, USA, [5]Now at National Institute of Water and Atmospheric Research, Wellington, Aotearoa New Zealand, [6]Energy and Environment Institute, University of Hull, Hull, UK, [7]Department of Earth Sciences, Durham University, Durham, UK

Key Points:

- Boulder-like detectors were developed to document the internal dynamics of sediment gravity flows
- Detectors were transported in 10 out of 14 sediment gravity flows that transited their locations in Monterey Canyon
- In each case, the body of the gravity flow consists of a faster dilute layer that overlies a slower denser basal layer

Supporting Information:

Supporting Information may be found in the online version of this article.

Correspondence to:

R. Gwiazda,
rgwiazda@mbari.org

Citation:

Gwiazda, R., Paull, C. K., Kieft, B., Klimov, D., Herlien, R., Lundsten, E., et al. (2022). Near-bed structure of sediment gravity flows measured by motion-sensing "boulder-like" Benthic Event Detectors (BEDs) in Monterey Canyon. *Journal of Geophysical Research: Earth Surface*, *127*, e2021JF006437. https://doi.org/10.1029/2021JF006437

Received 20 SEP 2021
Accepted 21 JAN 2022

Author Contributions:

Conceptualization: C. K. Paull, B. Kieft, D. Klimov, J. Xu, Katherine L. Maier, D. R. Parsons, Peter J. Talling
Data curation: R. Herlien, E. Lundsten, M. McCann
Formal analysis: R. Gwiazda, C. K. Paull, B. Kieft, M. McCann, Matthieu J. Cartigny, A. Hamilton
Funding acquisition: C. K. Paull, J. Xu, Katherine L. Maier, D. R. Parsons, Peter J. Talling
Investigation: R. Gwiazda, Matthieu J. Cartigny, A. Hamilton

© 2022. The Authors.
This is an open access article under the terms of the Creative Commons Attribution License, which permits use, distribution and reproduction in any medium, provided the original work is properly cited.

Abstract

The near-bed section of submarine gravity flows travels at the highest and most destructive speeds making direct measurements of this region of the flow difficult. Here results are presented from "boulder-like" Benthic Event Detectors (BEDs) that measured their own rotation, depth and temperature while carried within the near-bed region of gravity flows. BEDs were deployed in Monterey Canyon from 200 to 500 m water depth for 18 months (2016–2017) during the Coordinated Canyon Experiment. BEDs moved in 10 out of 14 gravity flows that transited the upper canyon. BEDs moved within the body of the flow because the initial velocities of the BEDs were 66 ± 16% (1 SD) of the flow transit velocities. BEDs rotated freely during most of their first moves and gained depth faster than in later moves, when their motion was more random and wobblier. The differences in BED motions between first and later moves suggest BEDs moved at different depths within the flow. The inferred near-bed flow structure is strongly stratified with a fast, less-dense layer moving above a slower and denser layer. Coherent changes between pressure and acceleration indicate that BEDs rode a crescent shaped bedform (CSB) morphology that persisted throughout flow events. The variability in BED speeds while riding the CSB morphology indicates a fluid-like nature of the near-bed layer. BED motions ended after being caught in the trough of a CSB. Based on recorded temperature decay rates after flow events, the thickness of redeposited sediment is 2–3 m.

Plain Language Summary

A large portion of the sediment discharged by rivers to the ocean is carried to the deep sea as sediment-laden currents, called sediment gravity flows, that are routed along submarine canyons carved on the continental slope. Because these flows are very energetic, episodic and occur in relatively inaccessible environments it has been challenging to document their velocity, sediment load, the thickness of the flow and internal structure, and the flow runout distance and duration. Boulder-shaped, motion-sensing devices, called Benthic Event Detectors (BEDs), were developed to better understand these flows. BEDs are capable of recording their own motion while being carried within sediment gravity flows. BEDs placed in Monterey Canyon for 18 months were carried by 10 sediment gravity flows. Based on the type of motion the BEDs experienced while being transported, it is inferred that the flows remobilize the seafloor down to 2–3 m and that the body of the flow behind the flow front consists of a very dense slow moving layer overridden by a fast less dense layer. Knowledge about the nature of these flows is important for evaluating the extent they constitute a geohazard to seafloor-resting infrastructure such as pipelines and seabed cables.

1. Introduction

Submarine canyons are an important link in the long-term global cycling of material on Earth. Sediment eroded on land is transported by rivers to the sea, where a large fraction is then carried into the deep ocean by near-seafloor sediment laden flows (called turbidity currents), which are routed through submarine canyons incised in continental slopes (Shepard, 1981). In addition, turbidity currents carry significant amounts of organic carbon that supports deep sea communities (Fernandez-Arcaya et al., 2017) and it is ultimately buried in deep sea fans (Galy et al., 2007; Mountjoy et al., 2018). Turbidity currents are also important from an economic perspective. Seabed cable networks that carry over 95% of global data traffic, as well as pipelines and other seabed

Methodology: R. Gwiazda, C. K. Paull, B. Kieft, D. Klimov, R. Herlien, J. Xu, Katherine L. Maier, D. R. Parsons, Peter J. Talling
Project Administration: R. Gwiazda, C. K. Paull, E. Lundsten, Katherine L. Maier, Peter J. Talling
Resources: R. Gwiazda, C. K. Paull
Software: B. Kieft, D. Klimov, R. Herlien, M. McCann, A. Hamilton
Supervision: C. K. Paull
Validation: B. Kieft, D. Klimov, A. Hamilton
Visualization: E. Lundsten, M. McCann
Writing – original draft: R. Gwiazda
Writing – review & editing: R. Gwiazda, C. K. Paull, E. Lundsten, Matthieu J. Cartigny, Katherine L. Maier, D. R. Parsons, Peter J. Talling

infrastructure, can be disrupted by these flows (Bruschi et al., 2006; Carter et al., 2014). Furthermore, deposits left behind by sediment-laden flows can host major oil reservoirs worldwide (Weimer & Link, 1991).

Submarine canyons are flushed by sediment flows driven by their excess density compared to the surrounding seawater. In this contribution, the term "sediment gravity flow" is used as the general name for these density-driven sediment transport events, whether they be low or high in sediment concentration, turbulent or laminar. Similar to rivers, but perhaps to a much larger degree, sediment transport along submarine canyons can be highly episodic, hence analogies between the two types of systems could be of interest. Sediment gravity flows in submarine canyons are triggered by a variety of factors that include: slope failures at the head of the canyon due to storms, wave action or tidal forcing (Ayranci et al., 2012; Bailey et al., 2021; Hughes Clarke, 2016), seawater density contrasts (Canals et al., 2006; Palanques et al., 2006), canyon-lip failure of rapidly accumulating sediment (Bailey et al., 2021; Carter et al., 2012; Flemings et al., 2008; Smith et al., 2007), direct hyperpycnal river discharge (Johnson et al., 2001; Liu et al., 2016; Parsons et al., 2001), and by submarine landslides due to earthquakes (Gavey et al., 2017; Heezen & Ewing, 1952; Mountjoy et al., 2018; Piper & Aksu, 1987). The scale of sediment gravity flows can vary greatly, but the largest events can carry exceptional volumes of sediment that may exceed the annual sediment flux from all of the world's rivers (Mountjoy et al., 2018; Talling, 2014; Talling et al., 2007).

Unpredictability in the timing of sediment gravity flows, coupled with their energetic character and the relative inaccessibility of submarine canyon channels, has made it difficult to study these flows in the field (Inman et al., 1976). Nevertheless, over the last 10 years, instrumental monitoring of sediment gravity flows has been accomplished successfully in a number of locations (Azpiroz-Zabala et al., 2017; Khripounoff et al., 2003; Hughes Clarke, 2016; Hughes Clarke et al., 2012; Zhang et al., 2018). One of these monitoring efforts was the Coordinated Canyon Experiment (Bailey et al., 2021; Heerema et al., 2020; Maier, Gales, et al., 2019; Maier, Rosenberger, et al., 2019; Paull et al., 2018; Wang et al., 2020) conducted in Monterey Canyon. This project monitored sediment gravity flows over a distance of ~50 km, from 285 to 1,850 m water depths, using an array of instrumented moorings and sensors on the seafloor. The proximity of the canyon head to shore facilitated frequent access using research vessels, allowing monitoring of the canyon conditions with a dense instrumental array at an unusually high temporal resolution.

Monterey Canyon is deeply eroded into the continental slope and shelf with the head of the canyon located a few hundred meters from shore (Figure 1a). Sediment sources include the Salinas River, smaller coastal rivers draining into and to the north of Monterey Bay, and cliff retreat. Littoral currents then carry this sediment, which may become trapped at the head of Monterey Canyon, where it accumulates until transported further down canyon (Bailey et al., 2021; Smith et al., 2007). Monitoring of Monterey Canyon prior to the CCE has shown that sediment gravity flows occur on a sub-annual basis and are very powerful (1.9 m s^{-1} velocity; Paull et al., 2002; Xu, 2010; Xu et al., 2004), having the capacity to destroy heavy instrument packages and carry very heavy objects over long distances (Paull et al., 2002, 2010). Repeat mapping of the upper canyon floor showed a dynamic environment consistent with upstream migration of crescent-shaped bedforms (CSB) taking place on a sub-annual basis (Paull et al., 2010; Smith et al., 2005, 2007; Xu et al., 2008).

In previous studies, the down canyon displacement of heavy objects (1,360 kg) by sediment gravity flows in Monterey Canyon was inferred from periodic tracking of their location (Paull et al., 2010). However, no information was collected about the motion of the objects during the flows or about the velocities of the flows. In Paull et al. (2018), based on CCE observations, it was concluded that sediment gravity flows in Monterey Canyon contained a dense basal near-seafloor layer that traveled at up to 7.2 m s^{-1} along the ocean floor ahead of a slower bottom water current carrying a suspended sediment load. The evidence for the presence of the basal layer included (a) the burial and exhumation of heavy objects in successive flows, (b) the mobilization of objects of different shapes and densities at similar speeds by the 24 November 2016 flow (Figure 4 in Paull et al., 2018), (c) the down canyon displacement of heavily anchored moorings, and (d) the faster flow transit (front) velocity compared to the maximum measured bottom current velocities.

Recently, modeling-based studies (Luchi et al., 2018) have proposed that turbidity currents with long runouts consist of two layers, with a dilute upper layer on top, and a highly concentrated fast layer underneath. Real time measurements of the lower part of the flow during sediment gravity flows could be useful to test this and other models (Parsons et al., 2007). In this contribution results are presented from Benthic Event Detectors (BEDs), which are new sensors designed to evaluate the near-seafloor conditions during sediment gravity flows. BEDs

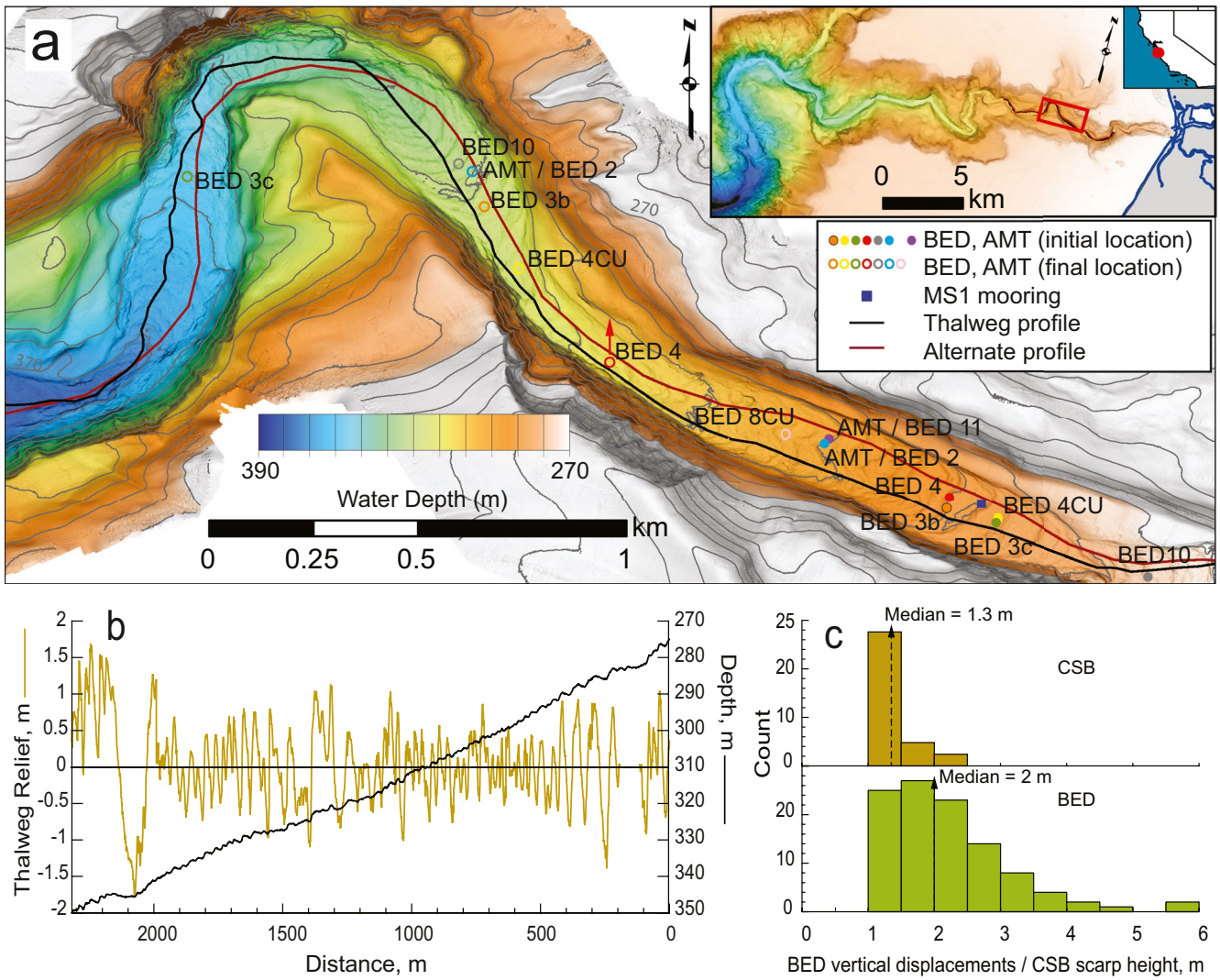

Figure 1. (a) Bathymetry of the upper section of Monterey Canyon, between 270 and 370 m, where most Benthic Event Detectors (BEDs) were carried by gravity flows. Inset show the location of map in a larger geographical context. Full circles are BED deployment locations, open circles are the last known BED positions. (Deployment locations of BED 5, 6a, 6b, 8CU, 9, and last known depths of BED 5, 6a, 6b, 9, Acoustic Monitoring Transponder are outside this map and shown on Figure 3.) BED 4 floated to the surface from the location shown by the red arrow, after being carried by the gravity flow of 1 December 2015. Initial BED velocities were calculated assuming that BEDs moved along the thalweg profile (red line) or an alternate profile along the channel edge (black line). Isobath at 10 m intervals. (b) Thalweg relief (left *y*-axis) is the residuals of the detrended thalweg between 275 and 350 mwd (right *y*-axis). (c) Comparison of the thalweg relief (> 1m) with BEDS rapid depth increases in the same depth range.

are seafloor-resting, motion-sensing instrument packages engineered to replicate the behavior of boulders in sediment gravity flows, while collecting information about their own motion. BEDs were deployed as part of the CCE instrument array that detected the passage of 15 sediment gravity flows over an 18 months period in 2016–2017. While the evidence for events propagating down canyon at speeds faster than the bottom water velocity was presented in Paull et al. (2018), the displacement of instrument packages was only discussed with reference to a sediment gravity flow event that occurred on 24 November 2016. In this new contribution, data are presented from all of the seafloor-resting platforms designed to monitor near-bed conditions, leading to new insights into near-bed processes and bedform evolution.

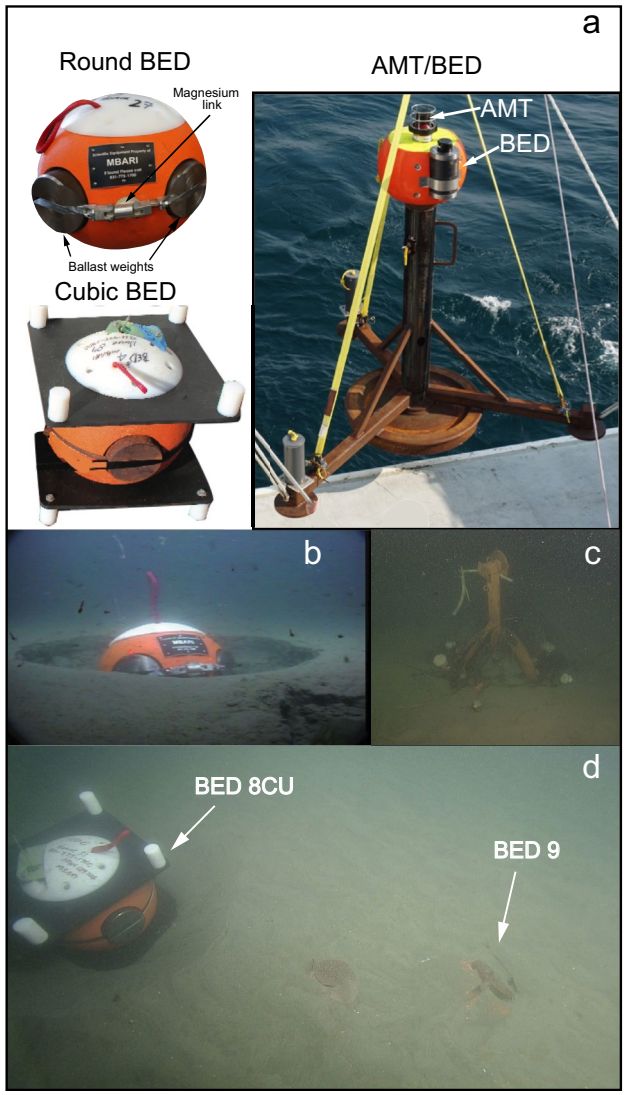

Figure 2. Photographs showing design and deployments of Benthic Event Detectors (BEDs). (a) Round and cubic BEDs, and Acousting Monitoring Transponder (AMT)/BED tripod frame. Only the electronic housing of a BED was attached to the tripod frame holding the AMT. (b) BEDs were typically deployed by placing them half-buried in the canyon floor. (c) AMT/BED 2 frame partially buried in the canyon floor when found on 26 April 2016. (d) BED 8CU when deployed on 5 October 2016, sitting on a remotely operated vehicle-made depression, next to BED 9 found buried after having moved during the sediment gravity flow of 1 September 2016.

1.1. Aims

The overarching goal is to understand the near-bed structure of sediment gravity flows from the unique information collected by the BEDs. In addition to showcasing the novelty and capability of these devices to monitor sediment gravity flows, the following specific questions are addressed:

1. *Sediment remobilization and flow thickness*: Does the seafloor sediment remobilize during sediment gravity flows? If so, to what depth is sediment remobilized per event?
2. *Location within the flow*: What part of the flow did BEDs record? The velocity of the flow varies in time and space. A comparison of the down canyon propagation velocity of the flow with the BEDs velocities provides an indication of what sections of the flow were monitored by the BEDs
3. *Flow structure*: What information can be gained about the flow structure from the type of motion experienced by the BED as they were carried by the flows? BEDs rotational behavior consisted of either pure rotation about an axis or a chaotic wobble/random motion. The circumstances under which BEDs adopted either type of rotation is utilized to infer the relative velocity and density of the flow surrounding the BED
4. *Shaping of the seafloor by sediment gravity flows*: The floor of Monterey Canyon is characterized by trains of crescent shaped bedforms (CSBs). Do CSBs persist and migrate upcanyon during sediment gravity flows? The pattern in the BEDs' angular accelerations as they moved down canyon is utilized to infer whether CSBs got obliterated or whether they persisted and migrated during sediment gravity flows.

2. Methods

2.1. Instruments

BEDs are instrument packages capable of recording their own motion placed inside engineered boulders. For the CCE, BEDs electronic components were housed inside a carbon fiber cylinder rated to 700 m water depth which was encased in spheres 0.42 m in diameter made of plastic and syntactic foam, and ballasted to a density of 1,770 kg m^{-3} by strapping iron weights around them (Figure 2a). BEDs weighed 81.5 kg in air and 35 kg in water. To evaluate whether an inability to roll could prevent BEDs from moving down canyon, two BEDs were modified into cubic shapes by adding top and bottom plates (Figure 2a). BEDs included a homer beacon (model 7815-000-06, Sonardyne, UK), which allowed a remotely operated vehicle (ROV) or surface vessel to find them, even when buried under 2 m of sediment according to field tests. Data were retrieved directly from the unit, if recovered, or via remote downloads through an onboard acoustic modem (model ATM-903, Teledyne Marine USA) that communicated to an autonomous surface vehicle or vessel at the surface.

The spheres did not have a spatially uniformly distributed mass. The belt of four ballast weights was positioned around a circumference of the sphere (Figure 2a). The pressure cylinder with batteries, motion sensor and electronic components was placed inside the sphere in an orientation perpendicular to the plane of the weights. Consequently, if allowed to freely roll, the sphere would rotate around a preferred axis of rotation determined by the uneven distribution of the moment of inertia. A corrodible magnesium link with an expected lifetime of half a year held the ballast weights strapped to the sphere. After the link dissolved, if the sphere was on the seafloor, it was expected to float to the surface to be recovered. BEDs were also equipped with an Argos customized SPOT

tag (Wildlife Computers Inc., USA) that combined Argos satellite tracking and VHF broadcast for RDF localization if they floated to the surface.

Each BED included an inertial motion sensor unit (IMU: MPU-6050, InvenSense, USA) consisting of 3-axis gyroscopes and 3-axis accelerometers; an internal temperature sensor (Microchip, TC1047A); and an interface for a pressure sensor (L'essor Français Electronique, model PHE163). The range of the accelerometers was ±16 g. The range of the gyroscopes was 2,000° s^{-1}. Data from both types of sensors were merged together to get calibrated sensor output and a fusion solution.

The data output of the BED was triaxial linear acceleration, orientation quaternion and pressure. BEDs monitored acceleration and orientation data continuously (1 kHz). Initiation of an event was identified by an increase in angular velocity above a threshold of 2° s^{-1}. Linear acceleration and orientation were saved at 50 samples per second until no motion was detected above the angular velocity threshold for longer than 2 s. Ambient pressure was sampled at 1 Hz, starting 5 s after the initiation of movement. When not in motion, data was recorded at a frequency of 1 sample every 10 min. After data download, pressure was converted to depth according to Fofonoff and Millard (1983), and the tide contribution to depth was subtracted using the mbotps routine of MB-systems (Caress & Chayes, 1996). To preserve battery capacity, motion data resolution was decimated to 5 Hz when wirelessly downloaded. The low-resolution temperature sensor recorded temperature within the pressure housing at a sampling rate of 1 measurement every 10 min. While originally designed to monitor the conditions of the electronic components, an unanticipated benefit was the somewhat muffled record of the temperature of the water and sediments surrounding the BED. These temperature records were retrieved only in the few instances where BEDs were physically recovered. BED battery life was typically about 1 year and heavily dependent on the frequency of data downloads.

A BED, along with an Acoustic Monitoring Transponder (AMT, Sonardyne, UK), was secured to the top of *a* > 2m tall 800 kg (in air) metal tripod with 1.5 m long legs (Figure 2a). The density of this platform is estimated at >6 kg m^{-3}. The AMT recorded pressure, temperature and tilt every 40 min, and these data were retrieved wirelessly by a surface vessel during the two AMT deployments.

2.2. BED Deployments

The experimental design of the CCE included continuous presence of BEDs on the canyon floor at 200, 300, and 400 m water depth. Within logistical constraints, after BEDs moved during sediment flows, these depths were repopulated with newly deployed or redeployed BEDs. A total of 11 BEDs and two AMT/BED deployments took place during the CCE (Figure 3). Most BEDs were deployed using MBARI's ROV *Ventana*. The ROV used a suction pump to dig a depression at preselected locations on the canyon thalweg into which the BED was placed half buried in the seafloor (Figure 2b). On two occasions, BEDs were deployed on the thalweg by letting them free-fall from the surface (BEDs 3b and 6b). The AMT/BED tripod was placed standing on the seafloor in both deployments. On the gravity flow of 15 January 2016, the AMT/BED 2 tripod moved ∼4.2 km down canyon, lost the BED, was found half buried in the seafloor (Figure 2c) and recovered by attaching a rope to it and winching it up to the *R/V Carson*. Depth and temperature records were retrieved from the still attached AMT. In the AMT/BED 11 tripod deployment the BED and AMT both remained attached to the frame. At the end of the study, the tripod was found almost completely buried and was not recoverable but BED 11 pressure and rotational data, and the AMT temperature record were retrieved via acoustic telemetry through the water column.

2.3. Data Processing

2.3.1. Velocities

Three types of velocities were evaluated: the maximum bottom water current velocity (V_{BW}), the transit velocity of the event (V_T), and the initial velocity of the BED ($V_{BED\,0}$). Near-bed current velocity (V_{BW}) was measured by an acoustic Doppler current profiler (ADCP) on mooring MS-1, which was positioned at approximately 300 m water depth (mwd) for almost the whole duration of the experiment (Figure 3; Paull et al., 2018). The downward looking 300 kHz ADCP was suspended 65 m above the seafloor, and collected a vertical profile of water velocity with a resolution of 1 m, every 30 s. The maximum velocity was defined as the maximum velocity measured by all four beams in at least one ping of the ensemble (Paull et al., 2018). During an event, the maximum velocity was

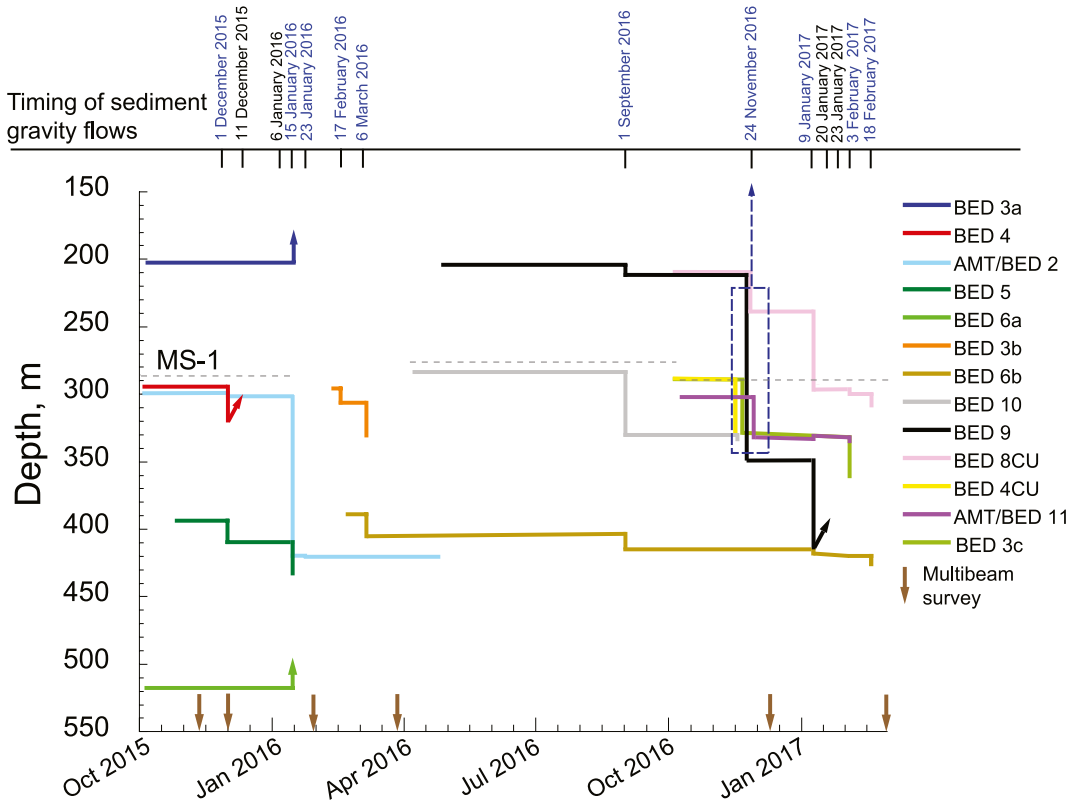

Figure 3. Locations (water depths) of the Benthic Event Detectors (BEDs) through time in Monterey Canyon during the CCE. BED 2 was lost when the Acoustic Monitoring Transponder/BED 2 moved during the 15 January 2016 event. The dates of sediment gravity flows during which BED moved are in blue along the top timeline; flows with no BED motions are in black. Arrows at the end of some lines indicate times when a BED in a gravity flow lost its weights, floated to the surface and was recovered. Dashed-blue rectangle shows BEDs that moved during the 24 November 2016 gravity flow. Horizontal dotted gray lines are depths of mooring MS-1 that held a downward-looking acoustic Doppler current profiler positioned 65 m above the seafloor during three deployments. The times of AUV multibeam surveys are noted with brown arrows.

between 1 and 4 m above the depth where the ADCP signal was fully attenuated. Under dilute flow conditions the depth of full attenuation would be the seafloor. But, at the beginning of the flow the depth of full attenuation moved upward due to the inability of the acoustic signal to penetrate the more concentrated flow.

The event transit velocity (V_T), is the average transit velocity of the flow between the preceding instrumental platform (up canyon mooring or BED) and the BED (Table 1). The average distance between the nearest up canyon instrumental platform and a BED was 3.2 km.

The initial BED velocity ($V_{\mathrm{BED}\,0}$) is defined here as the velocity of a BED from the initiation of movement until the average BED velocity changed. When plotted in coordinates of BED depth versus time, the average velocity change occurs at the point where the slope changes (Figure 4a).

In theory, the velocity could be calculated from the integration over time of the linear acceleration. However, the noisy signal of the motion sensor unit in addition to the sensor bias and the compounding error over time of the estimated velocity made this approach unworkable. Instead, for every episode of BED motion, $V_{\mathrm{BED}\,0}$ was obtained by comparing the trajectories (in distance-depth coordinates) of the BED at different possible velocities with bathymetric profiles of the canyon floor (Figure 4b). The velocity at which the BED trajectory most closely resembles the bathymetry was considered $V_{\mathrm{BED}\,0}$ (Figure 4c). The bathymetry profiles (one along the thalweg and one along the edge of the channel) were extracted from high resolution maps (1 m by 1 m by 0.25 m depth) that had been collected six times over the course of the CCE (Figures 1a and 3). The median difference in estimates of $V_{\mathrm{BED}\,0}$ using the thalweg profile and the edge of the channel profile was 0.3 m s^{-1}. The bathymetric map used for profile comparison was the survey collected most immediately prior to an event, except when there was another intervening event between survey and event (e.g., three events took place between the multibeam surveys of 7

Table 1
BEDs Velocities, Duration of Motion, Distances Traveled, and Distances Rotated

BED	Event	Type of motion, first (F) or later (L)	Initial velocity V_{BED} 0 (m s^{-1})	Event transit velocity to BED, V_T, (m s^{-1})	Duration of motion at V_{BED} 0 (s)	Distance traveled at V_{BED} 0 (m)	Duration of motion full event (s)	Total distance traveled (m)	Total distance rotated (m)	Total distance rotated/total distance traveled
4	1 December 2015	F	5.0	NA	41	205	230	679	389	0.57
5	1 December 2015	F	1.3	4.5	132	172	294	676	366	0.54
5	15 January 2016	L	5.0	6.8	57	284	539	972	318	0.33
3b	17 February 2016	F	2.6	NA	90	234	140	246	191	0.78
3b	6 March 2016	L	5.4	NA	83	446	266	846	357	0.42
6b	6 March 2016	F	3.2	4.8	80	254	203	581	249	0.43
9	1 September 2016	F	1.9	NA	74	137	101	226	149	0.66
10	1 September 2016	F	3.5	4.3	153	528	408	1,493	686	0.46
6b	1 September 2016	L	3.1	4.8	73	223	273	642	347	0.54
9	24 November 2016	L	2.3	NA	216	491	1,634	4,490	785	0.17
8CU	24 November 2016	F	3.2	NA	59	190	521	1,090	274	0.25
3c	24 November 2016	F	3.4	5.0	217	732	469	1,340	668	0.50
4 CU	24 November 2016	F	3.4	5.0	176	590	314	1,124	210	0.19
BED11/AMT	24 November 2016	F	3.5	5.0	98	338	248	989	20	0.02
10	24 November 2016	L	2.3	4.4	47	109	67	172	125	0.73
BED 8CU	9 January 2017	L	4.6	NA	110	501	546	1,773	302	0.17
9	9 January 2017	L	6.0	5.6	236	1,404	513	2,548	165	0.06
6b	9 January 2017	L	2.5	4.1	62	152	88	93	64	0.69
3c	3 February 2017	L	3.4	5.8	68	231	321	938	423	0.45
8CU	18 February 2017	L	3.0	NA	77	233	112	248	66	0.27

Note. BED, Benthic Event Detectors.

December 2016 and 21 February 2017 [Figure 3]). In those cases, $V_{BED\,0}$ is the average of the $V_{BED\,0}$ obtained from comparisons against profiles of the two bathymetric grids collected in the dates bracketing the event.

2.3.2. Rotation

BED rotational data consisted of orientation quaternions. A quaternion measurement describes the position of the BED relative to its initial position as a single rotation. It provides the coordinates of the axis of rotation, and the amount of rotation around the axis needed to arrive at the orientation of the BED from its initial position. After data download, a derived quaternion was calculated that represented the single rotation that occurred between two successive measurements (see Text S3 in Supporting Information S1). To visualize the BED motion and identify the periods when BEDs purely rotated or not, rotational data was converted into graphic animations (Data Set S1 in Supporting Information S1 [pure rotation], Data Set S2 in Supporting Information S1 [random/wobbling]). This involved the conversion of quaternion data into axis-angle rotation representations using the Python Euclid module available from the Python Package Index. This representation was then fed into an X3D scene graph rendered by the Spatial Temporal Oceanographic Query System web application (McCann et al., 2014; https://www.stoqs.org/).

The visual classification of motion as pure rotational or random/wobbling was verified by examining the orientation of the axis of rotation as the BED moved (Figure 5a). BED motion was classified as pure rotation if the orientation of at least 90% of the measured axes of rotations were within 40° of the orientation of the average axis of rotation over the time period examined (Figures 5b and 5c). Because of the uneven distribution of the BED mass, the preferential axis of rotation was expected to be perpendicular to the belt of ballast weights. Even when BEDs moved in a random/wobbling fashion this motion was quantified in units of rotations per second, which was done by adding the amount of rotation around an axis that changed position from measurement to measurement.

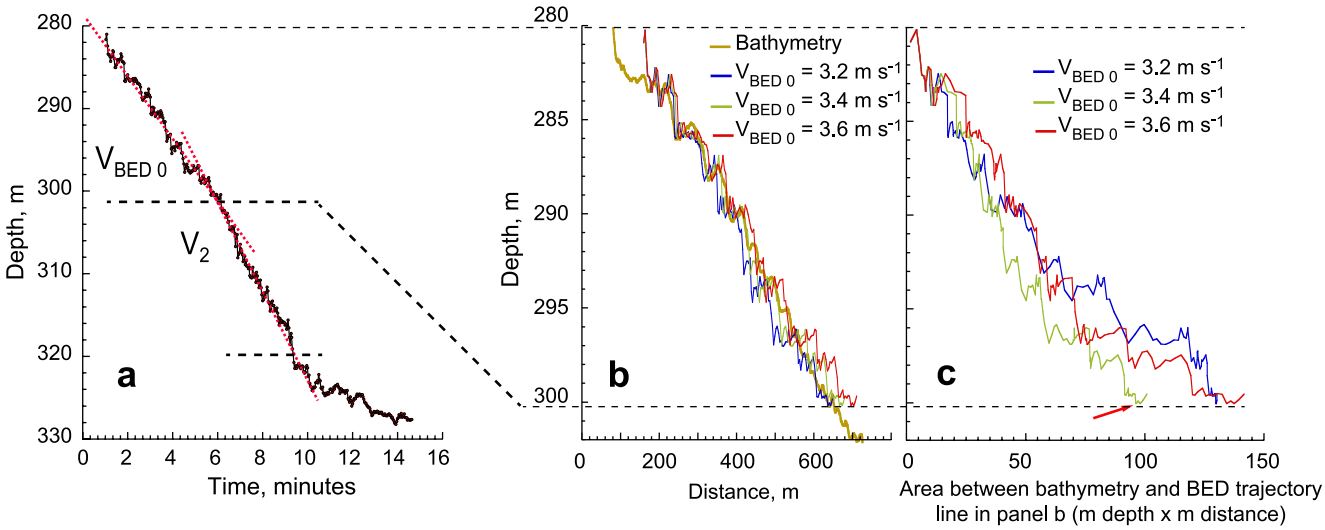

Figure 4. Approach to calculate $V_{BED\ 0}$, the initial velocity of a Benthic Event Detector (BED) when reached by a sediment gravity flow. (a) Change in depth with time of BED 10 immediately after being reached by the sediment gravity flow of 1 September 2016. A change in the velocity of the BED from $V_{BED\ 0}$ to V_2 is assumed to have taken place at the point where the average trend changes slope (red dotted lines). (b) Comparison of a bathymetry profile with the trajectory the BED would have followed at different velocities. (c) Cumulative areas in panel (b) between the bathymetry profile line and the BED trajectories lines of different velocities, as a function of depth. The red arrow indicates that for the depth range where the BED traveled at $V_{BED\ 0}$, the best fit (smallest cumulative area) between the BED trajectory and bathymetry profile corresponds to a velocity $V_{BED\ 0}$ of 3.4 m s^{-1}.

3. Results

Fourteen out of 15 gravity flows detected during the CCE transited through the BEDs depth range, in the uppermost section of the canyon (Paull et al., 2018). BEDs moved in 10 of those flows (Figure 3).

High frequency data recording of a newly deployed BED was always triggered by the first sediment gravity flow that reached that BED, and accompanying pressure increases indicated down canyon movement. After the first down canyon transit, BEDs did not always move when subsequent flow events passed the BED. No BED motions were recorded in four events (11 December 2015, 6 January 2016, 20 January 2017, and 23 January 2017, all indicated in Figure 3 in black font). In these four events there were no newly deployed BEDs in the canyon, only BEDs that had moved in previous events. Burial after motion was documented in a number of occasions when BEDs were located via their homer beacon (Figures 2c and 2d, Data Set S3 in Supporting Information S1). Even when the positions of buried BEDs were known from the homer beacon within a few meters, most attempts to recover them with an ROV failed because they were too deeply buried to be extracted from the seafloor.

3.1. Initial Motion Velocities

Considering all BEDs motions, a detectable change in the average initial velocity occurred between 41 and 236 s after the initiation of movement, while the total duration of BED motions ranged from 67 to 1,634 s. Thus, BEDs traveled at $V_{BED\ 0}$ for 40 ± 21% of the full BED movement duration. In that time, they covered 44 ± 23% of the total distance they traveled during the flow, suggesting that the velocity of the BED for the rest of the event did not differ much from $V_{BED\ 0}$.

BEDs moved at initial velocities $V_{BED\ 0}$ ranging from 1.3 to 6.0 m s^{-1} (Table 1, Figure 6). Event transit velocities V_T were measured over long distances (average = 3.2 km), but BED velocities $V_{BED\ 0}$ are closer to instantaneous velocities, as $V_{BED\ 0}$ were estimated over an average distance of 345 m. Except for one case (BED 9, 9 January 2017), the initial velocity of the BEDs was always lower than V_T, the event transit velocity. Overall, $V_{BED\ 0}$ were 66 ± 16% (1 SD) of the respective V_T. This proportion was independent of the magnitude of V_T, and appears to be independent of the shape and density of the BED. During the 24 November 2016 flow, the round BED, the cubic BED and the massive and denser ATM/BED 11 tripod all moved at close to the same initial velocity $V_{BED\ 0}$ (Figure 6).

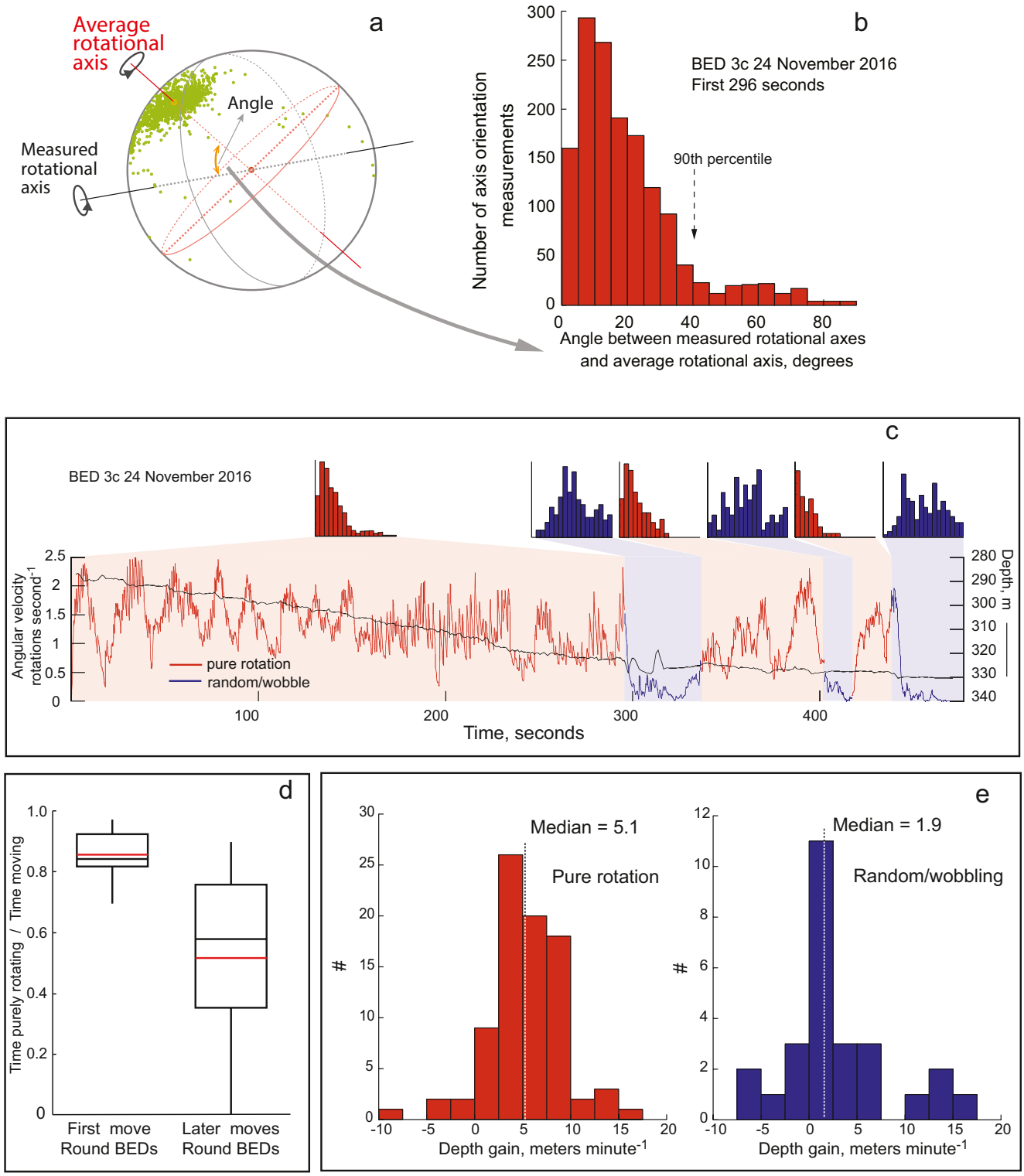

Figure 5. (a) Example showing how the variability in the orientation of the Benthic Event Detector (BED) axis of rotation was quantified. Each green dot indicates the orientation of the BED axis of rotation over a 0.2 s interval. The variability in the orientation of the axis of rotation is represented by the angle between each measured orientation and the average orientation throughout the period of time considered. (b) Histogram of the angle between each measurement and the average axis of rotation. If more than 90% of the measurements are within 40°, rotation is classified as purely rotational, otherwise as random/wobble. (c) Breakdown of the rotational motion of BED 3c on 24 November 2016 between purely rotational (red) and random/wobble (blue). (d) Box plot of time spent by round BEDs in purely rotational motion in their first move and in later moves. Red line is the median. (e) Depth gain when in purely rotational motion or in random/wobbling motion for all round BEDs. White dashed lines are median values.

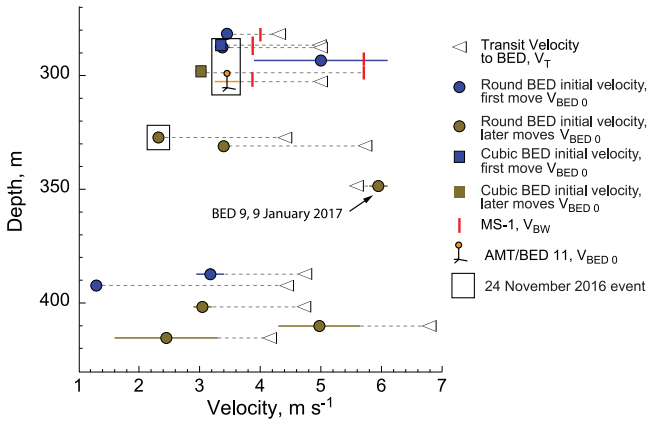

Figure 6. Comparison of the Benthic Event Detectors (BEDs) initial velocity ($V_{\text{Bed }0}$) with the transit (flow front) velocity of the flow (V_T) when it reaches the BED. The bottom current velocity (V_{BW}) measured at the MS-1 mooring at 300 mwd is also noted for those events where BEDs moved past the mooring. The rectangle indicates the motions that occurred during the gravity flow of 24 November 2016. Two shallower BEDs that moved during this event (BED 8CU and BED 9) are not shown because V_T at their depth could be not be determined. The solid color lines indicate the range in the BED velocity $V_{\text{Bed }0}$ estimates, based on the thalweg profile and channel edge profile (see Figure 1).

It is possible to compare the transit velocity of the event (V_T), the initial BED velocities ($V_{\text{BED }0}$), and the bottom water velocity (V_{BW}) in the instances when a sediment gravity flow transited past the ~300 mwd MS-1 mooring, which was equipped with a downward looking ADCP. This condition was met in five BED motions and once for the AMT tripod. For all but one of the instruments, it was their first move (Figure 3, BED 9 starting at 208 mwd not included for lack of comparable V_T). A comparison of the three velocities ($V_{\text{BED }0}$, V_{BW}, and V_T) shows that $V_T > V_{\text{BW}} > V_{\text{BED }0}$.

Whether BEDs moved or not did not appear to be strongly dependent on the velocity of the flows (Figure 6). Newly deployed BEDs and BEDs that had previously moved were carried by flows that moved at V_T as high as 6.8 m s^{-1} and as low as 4.1 m s^{-1}. No BED motions were recorded in four events: during the fastest of them, on 20 January 2017, with a V_{BW} of 5.4 m s^{-1}, there were five BEDs (8CU, 3c, ATM/BED 11 tripod, 4CU, 6b, Figure 3) in the canyon within the 294–420 m depth range that had moved in previous events, but none moved in this latter event. In two other flows (11 December 2015 and 6 January 2016), with V_{BW} <1.6 m s^{-1}, no BEDs moved. However, the mooring that recorded the bottom water velocity moved 3 m deeper in both events (equivalent to ~60 m lateral motion).

3.2. Down Canyon Transit

3.2.1. Rotation

BED rotational data were collected to distinguish the mode of transport of BEDs while traveling down canyon. Rotational motion was expected to be different if BEDs moved along the seafloor beneath a dilute suspended sediment load (where it was hypothesized they would roll), or if they were carried within a denser fluid (where motion may be less predictable and more random with reduced rotation rates).

The first down canyon movements of round BEDs were purely rotational for most of their trajectories (Figure 7). However, the BEDs did not simply roll over the seafloor because the distance traveled by rotation by round BEDs in their first move (including the latter sections where they moved with a random/wobble motion) was on average 56% of the total distance traveled (Table 1). Toward the end of their movement, the motion of BEDs switched to a wobbling/random motion, or alternated between rotation and wobbling before completely stopping. In the later moves of round BEDs, the alternation between pure rotation and random/wobbling occurs earlier and more frequently than in their first down canyon travel. The amount of time round BEDs spent in pure rotational motion was statistically significantly higher in first moves compared to later moves (*t*-test, $p < 0.03$, first moves: 85% of the time, later moves: 51% of the time, Figure 5d). Compared to round BEDs, cubic BEDs showed much more alternation between pure rotational and random/wobbling motion (Figure S2).

A faster increase in depth was observed when BEDs descended down canyon rotating (average of 5.1 m min^{-1}), compared to a descent with a random/wobbling motion (average of 1.9 m min^{-1}; Figure 5e, statistical significance $p < 0.0003$, Mann-Whitney U test). Because the canyon floor has a fairly constant slope (Paull, et al., 2011), the faster depth gain associated with rotation corresponds to BEDs moving at a faster velocity compared to when they moved with a random/wobble type of rotation. In addition, ~20% of the time the wobbling/random motion was associated not with a short-term depth gain but with a depth loss, that is, the BED climbed.

The type of rotation observed in the later moves of BED 9 (Figure 7, 24 November 2016, and 9 January 2017) is different from the rotational motions seen in all other round BEDs. No pure rotation, random or wobbling motion was observed. Instead, BED 9 traveled down canyon while experiencing a continuous rocking motion that never amounted to a full rotation (Data Set S4 in Supporting Information S1).

3.2.2. Trajectory Along the Canyon Floor

BEDs' trajectories include repetitive segments of slow depth gain followed by short and rapid depth increases (Data Set S1 in Supporting Information S1). This staircase pattern is most pronounced where CSBs are well

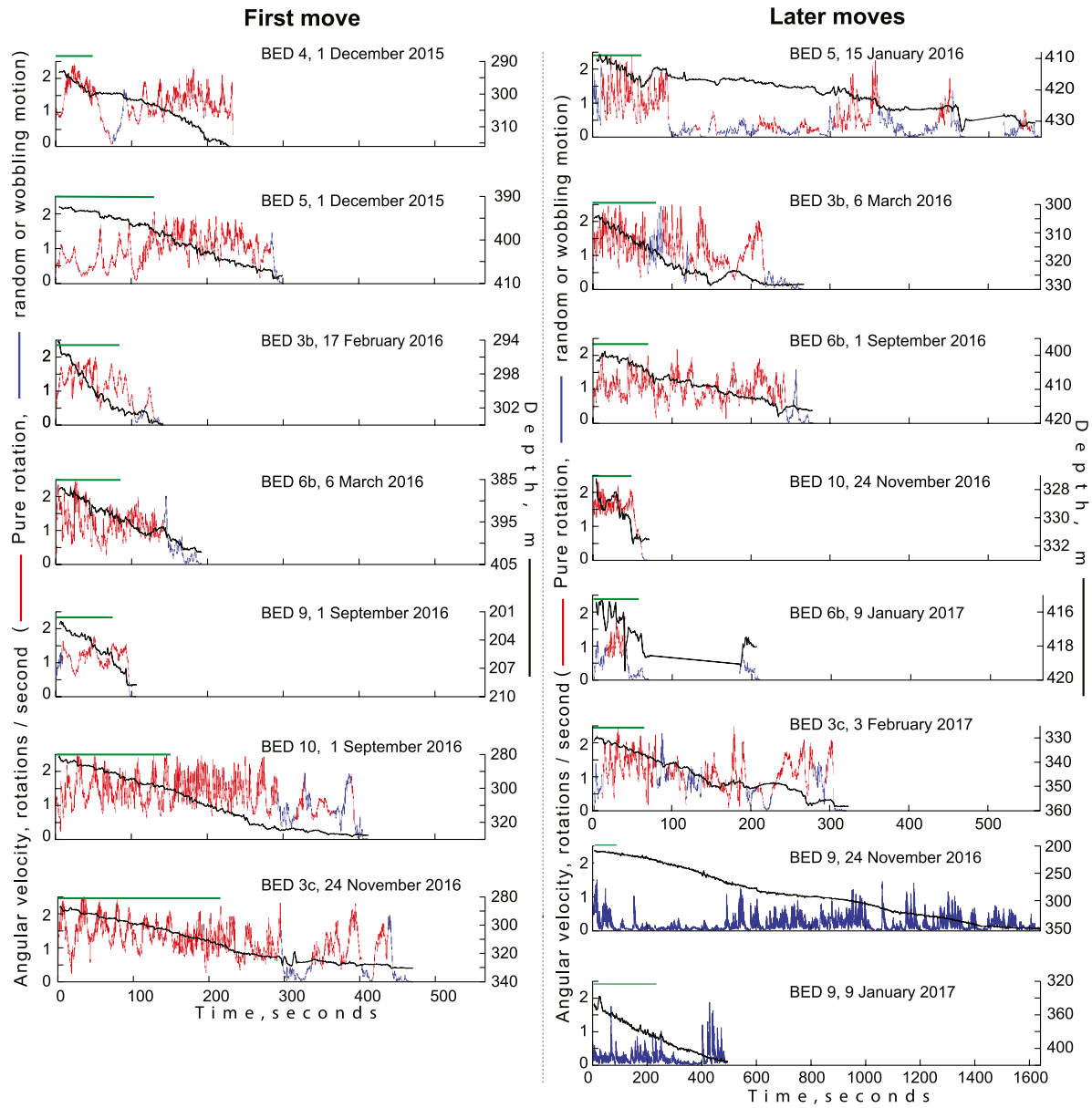

Figure 7. Round Benthic Event Detector (BEDs) rotational motion and depth versus time. First moves are in left column, later moves in right column. Depth in black, periods of pure rotational motion in red, random/wobbling in blue, except for BED 9 (24 November 2016 and 9 January 2017) that experienced a rocking motion without a single full rotation. Green line is the period over which initial velocity $V_{\mathrm{BED}\,0}$ was calculated for each BED.

developed along the canyon axis. The heights of the CSBs' scarps in the section of the canyon where most BEDs transited (275–350 mwd) was extracted from the detrended thalweg profile (Figure 1b) and compared to the BED rapid depth increases (Figure 1c). The comparison is limited to CSBs' scarps larger than 1 m because BEDs' vertical displacements smaller than 1 m may not be accurately detected given the BED 1Hz pressure sampling rate and the inherent error of the pressure sensor. The BEDs' rapid depth increases exceeded the maximum CSB topography amplitude 46% of the time, reaching a maximum 6 m height.

The relationship between the apparent topography ridden by the BEDs, as suggested by the BEDs' pressure changes, and the BEDs' angular acceleration maxima and minima was examined in a section of the canyon where CSBs are especially well developed, between 285 and 302 mwd (Figures 1b and 8). Angular acceleration maxima tend to align with the steeper sections of topography. Angular acceleration minima often immediately follow the angular acceleration maxima, such that maxima and minima are paired closely in time.

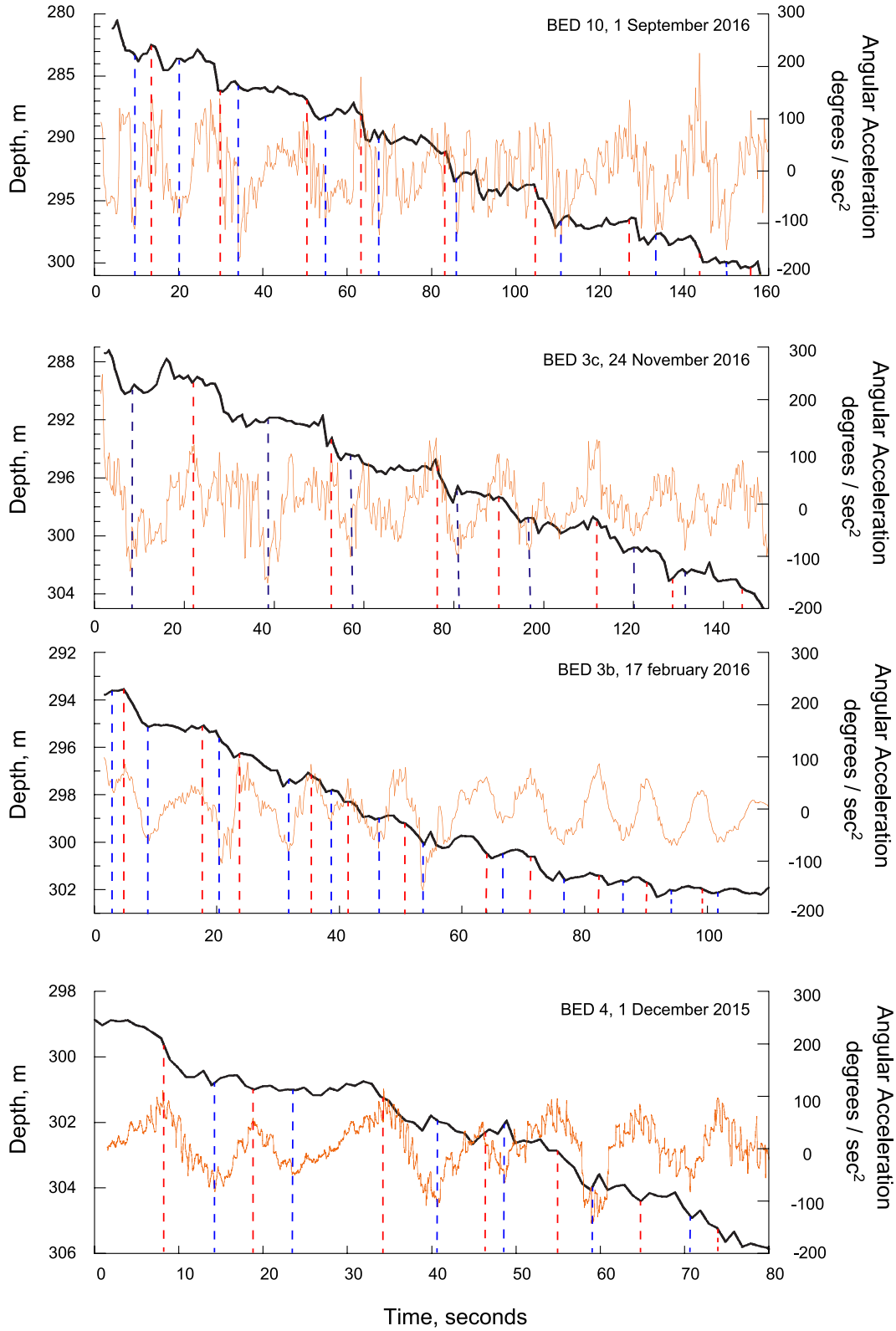

Figure 8. Record of angular acceleration (orange) and Benthic Event Detector (BED) depth (black) versus time of selected segments of the BEDs travel over sections of the canyon with well-developed crescent shaped bedforms. Red dashed lines are acceleration maxima and blue lines are minima (deceleration maxima). Angular acceleration was calculated over a running 3 s interval.

BED 9, in addition to traveling down canyon while experiencing a rocking motion not seen in other BEDs (Data Set S4 in Supporting Information S1), had both the longest, and the fastest down canyon transits of all BEDs. After a short first move during the sediment gravity flow of 1 September 2016, the BED was found buried (Figure 2d). It then moved again twice, first on 24 November 2016, and then on 9 January 2017 (Figure 3). The longest motion of all BEDs occurred during the 24 November 2016 event, when BED 9 traveled down canyon for 27 min over a distance of ∼4.5 km. During this event, while BED 9 was moving at 240 mwd with an average velocity of 1.25 m s^{-1}, the front of the flow reached BED 3c at 287 mwd, 1.3 km farther down canyon, at a speed of 5 m s^{-1}. The fastest BED motion occurred during the sediment gravity flow of 9 January 2017, when BED 9 $V_{\mathrm{BED}\,0}$ velocity of 6 m s^{-1} matched (within error) the transit velocity of the sediment flow (Figure 6).

3.3. End of Motion

Examination of the behavior of BEDs at the end of their motions can provide information about the conditions that lead to the cessation of a flow and deposition of its bed and suspended sediment load, and about the architecture of the sediment flow deposits that become the geologic record.

In the great majority of cases, the end of down canyon movement by a BED was preceded by a rapid increase in pressure (Figure 9). At the time of the fast increase in depth, and often before it, BEDs were rotating at a relatively high rate (≥1 rotation s^{-1}), either as pure rotation or with a random/wobbling motion. But with the rapid depth increase, the rotation velocity slows down considerably. In most cases, the decrease in BED rotational velocity is followed by a moderate shoaling of the BED. In a few cases, BEDs returned to the depth they were at prior to the sudden depth increase (Figure 9, plots within dashed lines). In all cases, the last moments of BED movement are not a pure-rotational motion coming to a gradual stop, but a continuous gentle wobble until all movement ends (Data Set S5 in Supporting Information S1). This sequence of events leading to the end of the BED down canyon travel is not noticeably different between round and cubic BEDs.

In many of the BEDs' trajectories, the magnitude of the depth increase prior to their end of motion is larger than the down canyon small-scale topography of the thalweg. Sixty-two percent (10 out 16) of the BEDs exhibited rapid depth increases before the end of motion that exceeded 2.2 m (the maximum amplitudes of the CSBs), reaching 7.6 m in the most extreme case.

3.4. Temperature

Temperature records exist only for the BEDs that were physically recovered (1 sample every 10 min) and for the AMT (1 sample every 40 min). The AMT had an oceanographic temperature sensor with a 0.01°C precision, 10 times better than the precision of the BED temperature sensor.

The BEDs recorded a decrease in average temperature each time a BED was reached by an event and moved into deeper, colder waters (Figure 10). In addition, the temperature displays a tide-related variability (Maier, Rosenberger, et al., 2019). A clear difference is seen in the BEDs' temperature variability before and after their first move. The temperature variability decreases to less than 50% of the variability prior to the first move, and it remains low after successive movements (Figure 10).

Part of the AMT temperature record was presented in Paull et al. (2018, their Figure 4d), and here it is shown in its totality (Figure 10). The temperature shows a tide-related variability after the AMT was deployed but the variability decreases or disappears after the AMT moved down slope with a gravity flow. In subsequent instances when the AMT was carried down canyon by a flow, the temperature suddenly increased and then decreased over the course of days to a stable value.

4. Discussion

The overarching aim of this paper it to understand the near-bed structure of sediment gravity flows from the information collected by these novel BEDs. To do this, we (a) evaluate the evidence for the existence of a near-seafloor basal dense layer, (b) identify where within the flow BEDS were carried, and (c) extract information about the

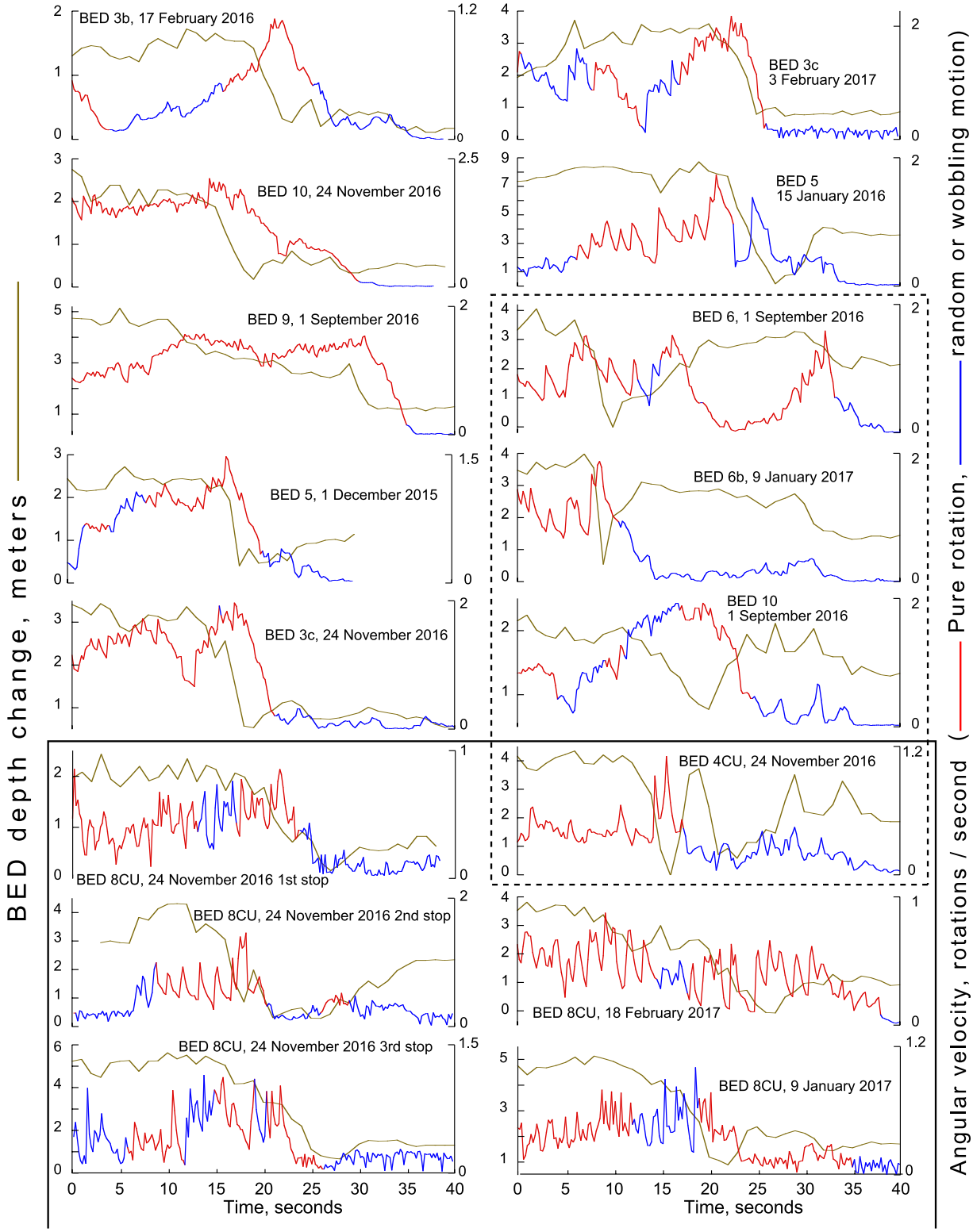

Figure 9. Benthic Event Detectors (BEDs) rotational motion and depth versus time at the end of BEDs motions. Depth in brown, periods of pure rotational motion in red, random/wobbling in blue. End of motion is preceded by a sudden depth increase. The four plots within the dashed rectangle are instances where BEDs ended their motion at the depth they were at prior to the sudden depth increase. Bottom six plots within solid rectangle are cubic BEDs.

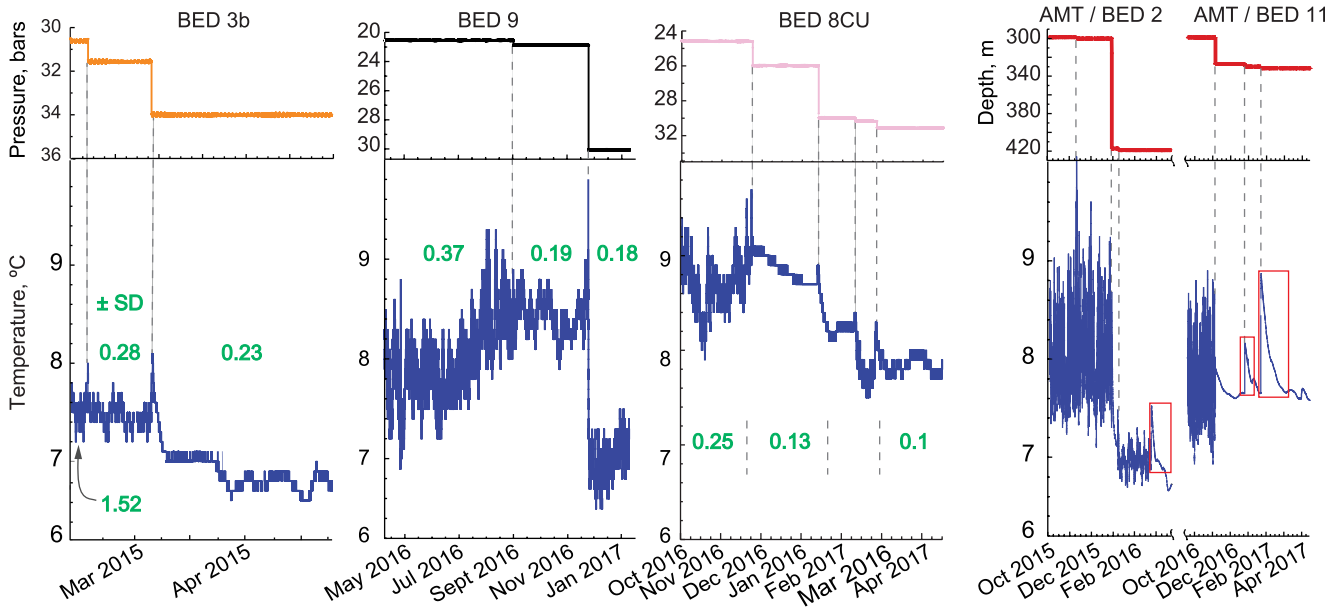

Figure 10. Changes in pressure/depth and temperature of Benthic Event Detectors (BEDs) that were physically recovered, and of the Acoustic Monitoring Transponder (AMT) frame. The green values inside the lower panes are the standard deviation of the temperature within the time defined by the vertical dashed lines. The red rectangles in the AMT temperature record are temperature decreases used to calculate the thickness of newly deposited sediment. Temperature record of AMT/BED 11 from Paull et al. (2018).

layer structure from the rotational motion of the BEDs. We also examine the consistency of the BEDs' angular acceleration and pressure changes with the migration of CSBs during gravity flows in the upper Monterey Canyon.

4.1. Evidence for Mobilization of the Seafloor

Over the course of the CCE, BEDs moved down canyon in 10 out of 14 sediment gravity flows in the 200–500 m water depth range. Nearly all BEDs moved more than once. The following evidence indicates that seafloor remobilization buried the BEDs after their first episode of movement. First, when BEDs were located with the ROV using their acoustic beacon, BEDs were found deeply buried, except for two instances when they were shallow enough for recovery (Figure 2c, Data Set S3 in Supporting Information S1). Second, the >2 m high AMT was found half-buried in the seafloor after its first deployment (Figure 2c), and almost fully buried after the second deployment (Figure S1a). Third, the variability in the tide-related temperature signal decreased after BEDs' first moves (Figure 10), consistent with the instruments having been removed from direct contact with water above the seafloor. Fourth, the fast flow of 20 January 2017 (V_{BW} of 5.4 m s^{-1}) did not carry any of the five BEDs that had moved earlier, consistent with the BEDs being buried too deeply for this flow to set them in motion. In addition, the deepening of heavily anchored moorings during gravity flow events (Paull et al., 2018), the faster down canyon propagation of the flows compared to their maximum measured bottom current velocities, and the mobilization of objects of different shapes and densities at the same speed in the 24 November 2016 flow event are all consistent with a remobilization of the seafloor. Lastly, studies involving heavy instrument packages deployed prior to the CCE documented up to 1.5 m burial after sediment gravity flows (Paull et al., 2010).

4.1.1. Thickness of Remobilized Sediment From Temperature Data

The remobilized sediment in a sediment gravity flow includes the dense flow and the up to 50 m thick dilute sediment cloud that followed it (Paull et al., 2018). Estimates of the thickness of the remobilized sediment after it stopped moving and settled can be calculated from the post-event AMT temperature signal decay, when available (Figure 10). The temperature evolution over time within the newly deposited sediment can be approximated as a solution to the heat conduction equation of a slab suddenly exposed at top and bottom to a different temperature (Carslaw & Jaeger, 1959; see Text S1 in Supporting Information S1 and Figure S1 for further details on this calculation).

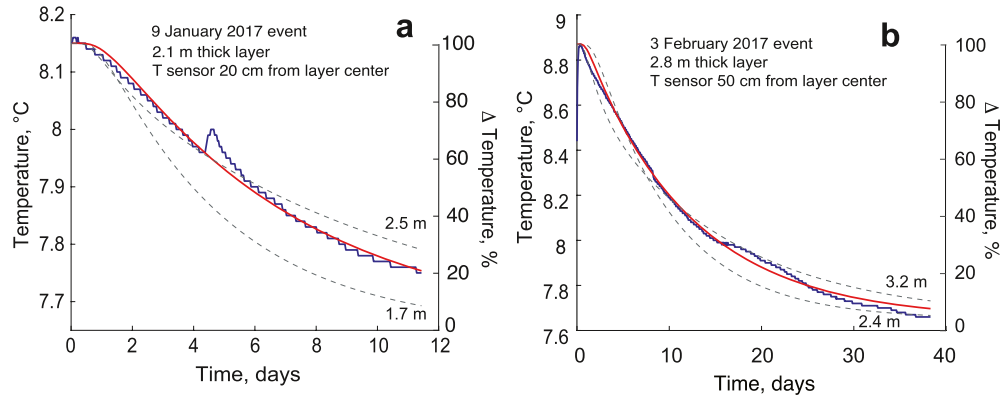

Figure 11. (a and b) Acoustic Monitoring Transponder temperature evolution post-9 January 2017, and post-3 February 2017 gravity flows (blue) and curve fits (red) according to the equation of heat conduction for a slab (see Text S1 in Supporting Information S1). Position of the sensor in the basal layer (20 in panel [a] and 50 cm in panel [b]) are fitted values, but they are minor modifiers of the fit as time to re-equilibration is mostly controlled by slab thickness (Figure S1c). Best fits correspond to layer thicknesses of 2.1 and 2.8 m. Dashed lines indicate the best fit that can be obtained when prescribing the layer to be 40 cm thicker or thinner and allowing the thermal conductivity to vary between 0.05 and 1×10^{-6} m^2 s^{-1}.

Sediment thicknesses of 2.5 m, 2.1 m and 2.8 m were obtained from the best fits to the post-event ATM temperature decays corresponding to the 24 November 2016, 9 January 2017, and 3 February 2017 events (Figure S1b, Figures 11a and 11b). This curve-fitting approach provides a well constrained estimate of the newly deposited sediment thickness. Allowing the sediment thickness to be 40 cm narrower or thicker renders a clearly worse fit to the temperature decay (Figures 11a and 11b).

The remobilized sediment thickness of 2–3 m is not dictated by the presence of bedrock at those depths below the thalweg. High-resolution seismic profiles of the upper canyon (Maier et al., 2018) indicate that the bedrock is located several tens of meters below the thalweg. If mobilized sediment traveled at a constant speed the shear stress at its base, calculated following the formulation of Mitchell, 2014, would have been in excess of 1,000 Pa, enough to erode cobbles or jointed bedrock through plucking. Instead the nearly consistent thickness of 2–3 m of mobilized sediment could result from a flow profile of decreasing velocity with depth.

4.2. BED Location Within the Flow

If it is assumed that the transit velocity of the event is the flow front velocity, the differences between the transit velocity of the event and BED velocities indicate that BEDs were translated behind and at a slower speed than the flow front. BEDs moved initially at velocities that were 66 ± 16% (1 SD) of the respective transit velocity of the event (V_T; Figure 6), and this proportion appears independent of the velocity of the flow and shape of the BED. The fast layer at the front sets in motion the newly and previously deployed BEDs (Figure 12), but the BEDs are incorporated into the trailing main body of the flow, moving at nearly constant and slower speeds than the flow front. Accordingly, BEDs recorded the conditions further back in the trailing body of the flow.

4.3. Flow Structure

The types of rotational motion experienced by the BEDs were not controlled by the small-scale morphology of the canyon floor because they typically persisted on the same type of motion over long distances (Figure 7). Here, it is proposed that the type of rotation is reflective of the speed and density of the flow behind the flow front. Pure rotation suggests that the near-bed flow is fast enough to move the BED, but not dense enough to prevent the BED from rolling unrestrained around its preferred axis of rotation. On the other hand, random/wobble rotational motion appears more consistent with a denser medium, perhaps even resembling a debris flow. The BED motion is then affected by turbulence exerted by the surrounding dense sediment-water mixture, forcing the axis of rotation to change orientation rapidly as a result of the forces acting from multiple directions. Differences in the type of rotation are accompanied by differences in down canyon velocity. When BEDs freely rotated, they not

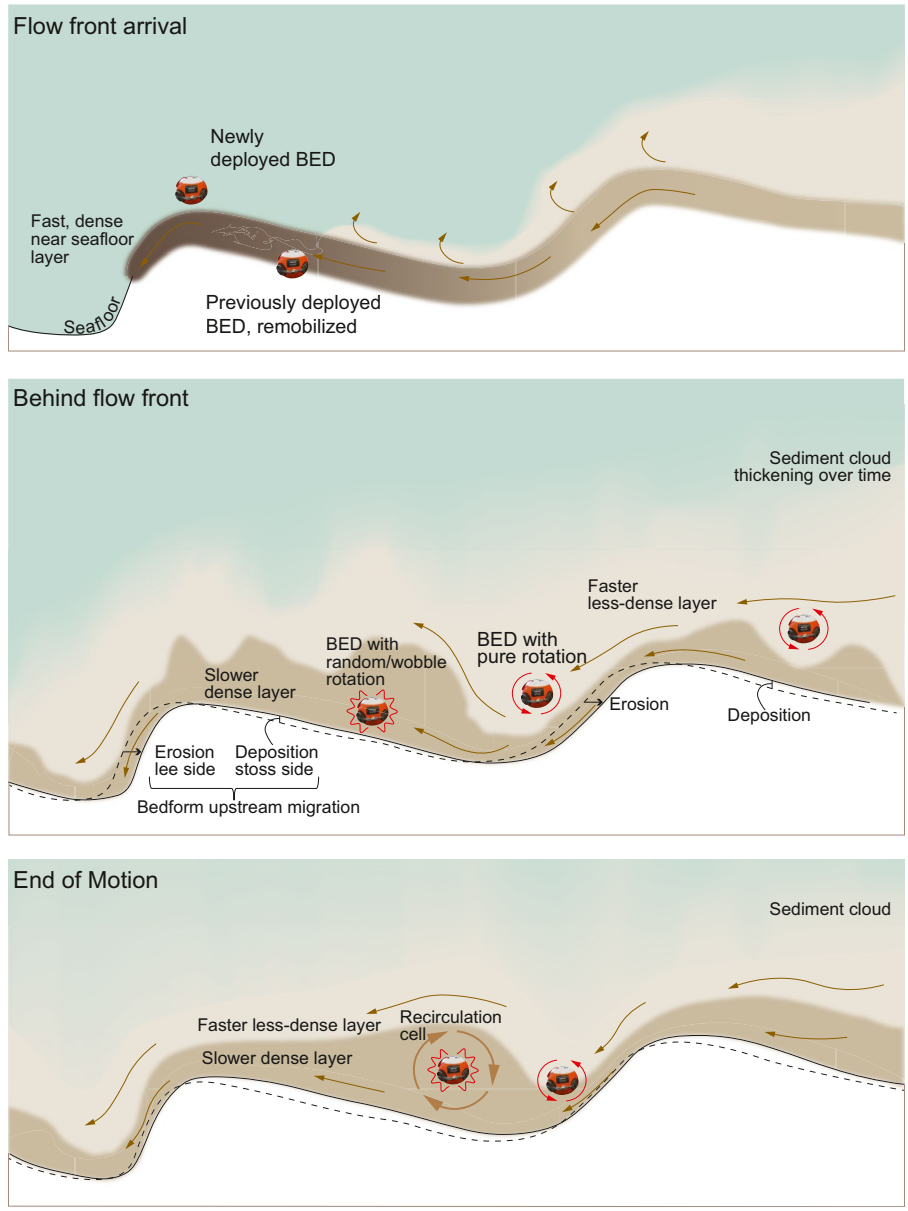

Figure 12. Schematic model of the Benthic Event Detector (BED) movement within a sediment gravity flow. Brown arrows are flow streamlines, red lines represent BED type of rotation, and dashed lines previous seafloor level.

only moved within a less dense fluid but also moved down-canyon at a faster speed than when they traveled with a random/wobble type of motion (Figure 5e).

The differences in type of rotation between BED's first and later moves can be interpreted in terms of a layered flow structure. BEDs' first moves started at or close to the seafloor, they freely rolled, and gained depth rapidly (Figures 5e and 7). BEDs' later moves started at a deeper level, were initiated by remobilization of the seafloor, and while they experienced both type of rotations, possibly due to vertical motion within the flow, they spent more time in random/wobble motion because they were within the denser part of the flow for longer (Figure 5d). Thus, the vertical layer structure behind the head of the flow includes a fast current where BEDs rolled, overriding a slow denser deeper level (Figure 12) where BEDs mostly wobbled. The possibility of an even deeper level not reached by the BEDs cannot be discounted. The interface between the two layers appears to be sharp because round BEDs spent significant amount of time, that is, longer than the travel time over a bedform, in pure rotational mode before switching to random/wobbling rotation (Figure 7). The upper level with the fast less dense flow is

further overlain by an even more dilute but slower sediment cloud up to 50 m thick that trails the two-layered main body of the flow (Paull et al., 2018; Wang et al., 2020).

4.4. Flow Thickness

Fast vertical displacements of BEDs as they moved down canyon provide an indication of the minimum thickness of the flow behind the flow front. The relief of the canyon floor includes up to 2.2 m amplitude bedforms, but the short-term vertical variability in BEDs' motions as they traveled down canyon exceeded this height, reaching 6 m (Figure 1c). This suggests the thickness of the flow body (some distance behind the flow front) may reach up to ~4 m (6.5–2.2 m). The larger range in BEDs' vertical displacements compared to the small-scale bathymetry relief indicates that BEDs moving with pure rotational motion are not simply rolling over the seafloor but rolling and moving vertically within a flow that carries them. The total distance BEDs rotated (first and later moves in either type of rotational motion) was on average 50% of the distance they traveled (Table 1), which further indicates BEDs were carried by the flow while they rolled within it. Because BEDs traveled over bedforms comprised of alternating steep and gentle slopes (Figure 12), they experienced short term fluctuations in velocity. Mass conservation dictates that the flow thickness changed to accommodate the velocity fluctuations (Dorrell et al., 2016).

In two instances, the vertical displacements in the BEDs' trajectories are of such large magnitude that they cannot be reconciled with movement along the thalweg relief. Plausible paths for BEDs that display these dramatic changes involve climbs along the canyon walls and a return to the channel, or cessation of motion along a terrace above the channel (Figure S3). In addition, the path of BED 9 includes long lasting (22 s) 17 m vertical displacement and repetitive short-term 3–5 m vertical displacements that cannot be matched to the canyon wall relief. Furthermore, BED 9 experienced both the longest (24 November 2016) and fastest (9 January 2017) travel of all BEDs while moving with a distinct rocking motion (Figure 7, Data Set S4 in Supporting Information S1). This unique behavior can be due to the BED having become ensnared with debris (e.g., trash, fishing gear, and kelp) that acted as a sail and prevented it from moving freely. During the fast event of 9 January 2017, the BED velocity matched the speed of the event, suggesting it moved within the flow front, while having short-term vertical displacements of up to 5 m compared to a seafloor relief of <1.5 m. However, because of the suspected entrapment with debris, 5 m vertical displacements could be the maximum vertical motion allowed by its attachment to the debris entrained within the flow, and not an indication of the flow thickness. Entrainment with debris carried by the flow could also account for the long travel the BED had on 24 November 2016.

The behavior of the BEDs at the end of their travel provides additional information about the flow thickness. The end of motion is preceded by a relatively abrupt increase in pressure (depth) and a switch in rotational motion from pure rotation to random/wobble (Figures 9 and 12). In the majority of cases (62%) the steep depth increase exceeds the maximum amplitude of the CSBs (2.2 m) reaching up to 6–7 m, providing further evidence that the thickness of the flow can be as high as ~4 m. The pressure increase prior to the end of motion is not due to rapid piling of sediment above the BED at the same water depth because the thickness of sediment that would account for the observed pressure increases is too large. For example, if a pressure increase equivalent to 2 m deepening, inferred for the moderate pressure gains of some of the BEDs at the end of motion (Figure 9), were only due to the added weight of rapid (<10 s) sediment piling, a fast accumulation of 4 m of a sediment slurry (density = 1.5 g cc^{-1}) would be needed to account for the fast pressure change. Instead, the sharp increase in depth is interpreted as the descent of the BED along the lee side of a bedform into the trough that precedes a hydraulic jump. At this transition, the flow velocity decreases, the flow thickness increases leading to a pronounced reduction of flow shearing rate (Garcia & Parker, 1989; Postma et al., 2009). The presence of a recirculation cell immediately before the hydraulic jump, as documented in stratified density driven gravity flows (Dorrell et al., 2016), could further hinder the BED advancement. It is also possible that when the BED descended along the lee side of the bedform, it also dipped into a deeper level of the flow that is denser and slower, contributing to the BED deceleration. The BED motion ends after the rotational motion switches from purely rotation to a random wobble and, lacking enough momentum to overcome the hydraulic jump, it stops.

4.5. Crescent Shaped Bedform Persistence and Migration

Up canyon migration of the ubiquitous trains of CSBs observed along the canyon floor has been hypothesized on the basis sub-annual repeated bathymetric surveys which showed different spatial arrangements of CSBs

between surveys (Paull et al., 2011; Smith et al., 2005, 2007). Repeat high-resolution mapping during the CCE of the section of the canyon where BEDs were deployed provides strong evidence that up canyon migration of CSBs indeed takes place (Data Set S6 in Supporting Information S1). In some instances, for example, during the most powerful event of the CCE on 15 January 2016, it is uncertain whether CSBs were partly destroyed. Subsequent surveys show CSBs resumed up canyon migration. The thickness of the newly deposited sediment in the three events (2.1–2.8 m) calculated on the basis of the AMT temperature decays is comparable to the maximum amplitude of the bedforms in the canyon floor between 275 and 350 m (2.2 m), and the thickness of remobilized seafloor (<3 m) measured by repeated high resolution mapping.

This up canyon migration direction supports the interpretation that CSBs are the morphological expression of cyclic step instabilities. They form as a result of an alternation of the flow along the seafloor between supercritical (Froude number >1) and subcritical (Froude number <1; Cartigny et al., 2011; Kostic, 2011; Slootman & Cartigny, 2020; Sumner et al., 2013; Winterwerp et al., 1992). At the transition between the two types of flow there is a hydraulic jump, that is, a thickening and sharp deceleration of the flow. The seafloor morphology reflects the down canyon evolution of the flow velocity. The steep side of the bedforms is where the flow is supercritical. It accelerates and erodes the seafloor resulting in the upcanyon migration of the bedform. At the bottom of the lee side the flow decelerates and becomes subcritical, creating a hydraulic jump. As the flow continues along the stoss side at a lower velocity, sediment is deposited or less sediment is eroded compared to the lee side.

The behavior of the BEDs along the sections of the canyon where the CSBs are most prominent is consistent with the BEDs riding a CSB morphology (Figure 8). BEDs' angular acceleration maxima tend to be associated with the steep increases in BED depth, as expected if the BED was descending along the lee side of a CSB. A BED angular acceleration minimum (deceleration maximum) closely following an acceleration maximum is consistent with the BED decelerating quickly as it moves through a hydraulic jump. A slow acceleration accompanied by a moderate change in depth follows, suggesting a gradual gain in speed as the BED continues its motion along the stoss side of the CSB.

The coherent changes between BED velocity and topography are consistent with the fluid nature of the body of the flow as indicated by the up canyon migration of the bedforms. A non-fluid slab could not accommodate deceleration with expansion in bedform troughs, and acceleration with thinning toward the bedform crest. The vertical structure of the flow suggested by the BEDs' rotational data further indicates that the fluid layer includes a dense slower level and a fast less dense upper level.

While the BED data are useful for gaining insights into the dynamics of the body of the flow, questions remain about the nature of the flow front. The estimated thickness of the body of the flow, where BEDs were carried, was at most 4 m. However, CSBs with a maximum amplitude of 2.2 m were not wiped out by the advancing flow, which included a dense near-bed layer. A possible interpretation of this observation is that the thickness of the flow front and of the dense near-bed layer in the main body of the flow are smaller than the amplitude of the bedforms.

4.6. Crescent Shaped Bedform Stratigraphic Structure

It is not clear what is the sediment structure of a CSB formed by a mobilized seafloor layer. Cores recovered prior to the CCE along a downstream longitudinal profile of several bedforms (Paull et al., 2010) contain sequences with poorly sorted intervals of gravel and clay clasts near the base, overlain by fining upwards sand. However, no systematic variations were noted along the transect that relate the core stratigraphy with the core position along the CSB. The longest core was 1.8 m but many cores were ∼1 m or shorter. Given than the thickness of freshly deposited sediment is in the order of 2–3 m, as indicated by the AMT temperature record (Figures 11a and 11b, Figure S1b), it is possible that the core record is not complete enough to capture the full stratigraphy of CSB deposits. No evidence for net erosion or aggradation over the course of the CCE was detected by high resolution mapping of Monterey Canyon's thalweg. This would indicate that each incoming flow eroded to some extent the sedimentary record of previous flows through CSBs migration. A robust flow would leave untouched only the deepest filled scours of previous events (Hage et al., 2018).

Buried instruments were exhumed by the advancing flow front, and by the sediment remobilization associated with the up canyon migration of CSBs. The lack of motion of buried BEDs in some of the events can be due to the combination of BEDs having been buried deeper than the thickness of the remobilized sediment, and having

not yet been eroded out by the retrograde migration of a bedform lee side. Some events may have died out at water depth shallower than where the instruments were located.

5. Conclusions

Boulder-like detectors capable of recording their depth, rotational motion and temperature were placed in Monterey Canyon for 18 months in 2016–2017 between 200 and 400 mwd. The detectors were carried by 10 sediment gravity flows. Remobilization of the seafloor took place in all flows. Because initially BEDs moved at velocities that were 66 ± 16% (1 SD) of the transit velocity of the event, BEDs moved within the main body of the flow behind the flow front. In their first move, BEDs mostly rotated around a preferred axis of rotation. In later moves, after they have been buried by the preceding flow, in addition to rotation around a preferred axis, their rotation also included a larger proportion of periods with random/wobble motion.

The combined depth and rotational data from the BEDs is consistent with the existence of a near seafloor dense basal layer in sediment gravity flows in Monterey Canyon, as proposed in Paull et al. (2018). The interpretation of the BEDs' rotational data is that at least behind the flow front, the near-bed layer is not a uniform sediment slab with well-defined upper and lower boundaries, but a fluid layer of varying thickness that accommodates changes in velocity caused by a variable seafloor morphology and bedforms. The lowest level of the layer is dense and slow. Higher in the flow, the flow is faster and less dense, without a well-defined upper boundary. The post-event temperature decay rates, measured in instruments buried by gravity flows, are consistent with a thickness of remobilized seafloor sediment in the order of 2–3 m. The short term vertical variability of BEDs motions while traveling down canyon exceeded the thalweg crescent shaped bedforms' vertical relief by up to 4 m, suggesting this is the upper limit for the thickness of the double-layered main body of the flow. Coherent changes between the BEDs' angular acceleration and pressure indicate that BEDs moved downcanyon while riding a crescent shaped morphology that persisted throughout the gravity flows.

Data Availability Statement

All BEDs pressure and rotational data and AMT temperature records are available at the Marine Geoscience Data System data repository, https://doi.org/10.1594/IEDA/324759. A graphical user interface (GUI) is available through the portal https://stoqs.mbari.org/stoqs_cce2015. Instructions on how to use this GUI to visualize the complete set of BEDs' motions animations, and to access rotational motion-related parameters are in the Supporting Information S1.

Acknowledgments
The David and Lucile Packard Foundation, the Natural Environment Research Council (NE/K011480/1 and NE/L013142/1), the U.S. Geological Survey, the Ocean University of China, and the Qingdao National Laboratory for Marine Science and Technology, provided support. D. R. Parsons received additional funding through EU Horizon 2020 Programme (GEOSTICK, Grant 725955). Thanks to the R/Vs *Western Flyer*, *Rachel Carson* and *Paragon* crews, ROV pilots and AUV operators. Reviews by John Hughes Clarke, Neil Mitchell, and an anonymous reviewer helped to improve this manuscript.

References

Ayranci, K., Lintern, D. G., Hill, P. R., & Dashtgard, S. E. (2012). Tide-supported gravity flows on the upper delta front, Fraser River delta, Canada. *Marine Geology*, *326–328*, 166–170. https://doi.org/10.1016/j.margeo.2012.09.007

Azpiroz-Zabala, M., Cartigny, M. J. B., Talling, P. J., Parsons, D. R., Sumner, E. J., Clare, M. A., et al. (2017). Newly recognized turbidity current structure can explain prolonged flushing of submarine canyons. *Science Advances*, *3*(10), e1700200. https://doi.org/10.1126/sciadv.1700200

Bailey, L. P., Clare, M. A., Rosenberger, K. J., Cartigny, M. J. B., Talling, P. J., Paull, C. K., et al. (2021). Preconditioning by sediment accumulation can produce powerful turbidity currents without major external triggers. *Earth and Planetary Science Letters*, *562*, 116845. https://doi.org/10.1016/j.epsl.2021.116845

Bruschi, R., Bughi, S., Spinazzè, M., Torselletti, E., & Vitali, L. (2006). Impact of debris flows and turbidity currents on seafloor structures. *Nowegian Journal of Geology*, *86*, 317–337.

Canals, M., Puig, P., de Madron, X. D., Heussner, S., Palanques, A., & Fabres, J. (2006). Flushing submarine canyons. *Nature*, *444*(7117), 354–357. https://doi.org/10.1038/nature05271

Caress, D. W., & Chayes, D. N. (1996). Improved processing of Hydrosweep DS multibeam data on the R/V Maurice Ewing. *Marine Geophysical Researches*, *18*(6), 631–650. https://doi.org/10.1007/BF00313878

Carslaw, H. S., & Jaeger, J. C. (1959). *Conduction of heat in solids* (2nd ed.). Oxford University Press.

Carter, L., Gavey, R., Talling, P., & Liu, J. (2014). Insights into submarine geohazards from breaks in subsea telecommunication cables. *Oceanography*, *27*(2), 58–67. https://doi.org/10.5670/oceanog.2014.40

Carter, L., Milliman, J. D., Talling, P. J., Gavey, R., & Wynn, R. B. (2012). Near-synchronous and delayed initiation of long run-out submarine sediment flows from a record-breaking river flood, offshore Taiwan. *Geophysical Research Letters*, *39*(12). https://doi.org/10.1029/2012GL051172

Cartigny, M. J. B., Postma, G., van den Berg, J. H., & Mastbergen, D. R. (2011). A comparative study of sediment waves and cyclic steps based on geometries, internal structures and numerical modeling. *Marine Geology*, *280*(1), 40–56. https://doi.org/10.1016/j.margeo.2010.11.006

Dorrell, R. M., Peakall, J., Sumner, E. J., Parsons, D. R., Darby, S. E., Wynn, R. B., et al. (2016). Flow dynamics and mixing processes in hydraulic jump arrays: Implications for channel-lobe transition zones. *Marine Geology*, *381*, 181–193. https://doi.org/10.1016/j.margeo.2016.09.009

Fernandez-Arcaya, U., Ramirez-Llodra, E., Aguzzi, J., Allcock, A. L., Davies, J. S., Dissanayake, A., et al. (2017). Ecological role of submarine canyons and need for canyon conservation: A review. *Frontiers in Marine Science*, *4*. https://doi.org/10.3389/fmars.2017.00005

Flemings, P. B., Long, H., Dugan, B., Germaine, J., John, C. M., Behrmann, J. H., et al. (2008). Pore pressure penetrometers document high overpressure near the seafloor where multiple submarine landslides have occurred on the continental slope, offshore Louisiana, Gulf of Mexico. *Earth and Planetary Science Letters*, *269*(3), 309–325. https://doi.org/10.1016/j.epsl.2007.12.005

Fofonoff, N. P., & Millard, R. C. (1983). Algorithms for computation of fundamental properties of seawater. Endorsed by Unesco/SCOR/ICES/IAPSO Joint Panel on Oceanographic Tables and Standards and SCOR Working Group 51. Unesco Technical Papers in Marine Science, No. 44.

Galy, V., France-Lanord, C., Beyssac, O., Faure, P., Kudrass, H., & Palhol, F. (2007). Efficient organic carbon burial in the Bengal fan sustained by the Himalayan erosional system. *Nature*, *450*(7168), 407–410. https://doi.org/10.1038/nature06273

Garcia, M., & Parker, G. (1989). Experiments on hydraulic jumps in turbidity currents near a canyon-fan transition. *Science*, *245*(4916), 393–396. https://doi.org/10.1126/science.245.4916.393

Gavey, R., Carter, L., Liu, J. T., Talling, P. J., Hsu, R., Pope, E., & Evans, G. (2017). Frequent sediment density flows during 2006 to 2015, triggered by competing seismic and weather events: Observations from subsea cable breaks off southern Taiwan. *Marine Geology*, *384*, 147–158. https://doi.org/10.1016/j.margeo.2016.06.001

Hage, S., Cartigny, M. J. B., Clare, M. A., Sumner, E. J., Vendettuoli, D., Hughes Clarke, J. E., et al. (2018). How to recognize crescentic bedforms formed by supercritical turbidity currents in the geologic record: Insights from active submarine channels. *Geology*, *46*(6), 563–566. https://doi.org/10.1130/G40095.1

Heerema, C. J., Talling, P. J., Cartigny, M. J., Paull, C. K., Bailey, L., Simmons, S. M., et al. (2020). What determines the downstream evolution of turbidity currents? *Earth and Planetary Science Letters*, *532*, 116023. https://doi.org/10.1016/j.epsl.2019.116023

Heezen, B. C., & Ewing, W. M. (1952). Turbidity currents and submarine slumps, and the 1929 Grand Banks [Newfoundland] earthquake. *American Journal of Science*, *250*(12), 849–873. https://doi.org/10.2475/ajs.250.12.849

Hughes Clarke, J. E. (2016). First wide-angle view of channelized turbidity currents links migrating cyclic steps to flow characteristics. *Nature Communications*, *7*(1), 1–13. https://doi.org/10.1038/ncomms11896

Hughes Clarke, J. E., Brucker, S., Muggah, J., Church, I., Cartwright, D., Kuus, P., et al. (2012). The Squamish ProDelta: Monitoring active landslides and turbidity currents. In *Canadian Hydrographic Conference 2012, Proceedings* (p. 15).

Inman, D. L., Nordstrom, C. E., & Flick, R. E. (1976). Currents in submarine canyons: An air-sea-land interaction. *Annual Review of Fluid Mechanics*, *8*(1), 275–310. https://doi.org/10.1146/annurev.fl.08.010176.001423

Johnson, K. S., Paull, C. K., Barry, J. P., & Chavez, F. P. (2001). A decadal record of underflows from a coastal river into the deep sea. *Geology*, *29*(11), 1019–1022. https://doi.org/10.1130/0091-7613(2001)029<1019:adrouf>2.0.co;2

Khripounoff, A., Vangriesheim, A., Babonneau, N., Crassous, P., Dennielou, B., & Savoye, B. (2003). Direct observation of intense turbidity current activity in the Zaire submarine valley at 4000 m water depth. *Marine Geology*, *194*(3), 151–158. https://doi.org/10.1016/S0025-3227(02)00677-1

Kostic, S. (2011). Modeling of submarine cyclic steps: Controls on their formation, migration, and architecture. *Geosphere*, *7*(2), 294–304. https://doi.org/10.1130/GES00601.1

Liu, J. T., Hsu, R. T., Hung, J.-J., Chang, Y.-P., Wang, Y.-H., Rendle-Bühring, R. H., et al. (2016). From the highest to the deepest: The Gaoping River–Gaoping submarine canyon dispersal system. *Earth-Science Reviews*, *153*, 274–300. https://doi.org/10.1016/j.earscirev.2015.10.012

Luchi, R., Balachandar, S., Seminara, G., & Parker, G. (2018). Turbidity currents with equilibrium basal driving layers: A mechanism for long runout. *Geophysical Research Letters*, *45*(3), 1518–1526. https://doi.org/10.1002/2017GL075608

Maier, K. L., Gales, J. A., Paull, C. K., Rosenberger, K., Talling, P. J., Simmons, S. M., et al. (2019). Linking direct measurements of turbidity currents to submarine canyon-floor deposits. *Frontiers of Earth Science*, *7*. https://doi.org/10.3389/feart.2019.00144

Maier, K. L., Johnson, S. Y., & Hart, P. (2018). Controls on submarine canyon head evolution: Monterey Canyon, offshore central California. *Marine Geology*, *404*, 24–40. https://doi.org/10.1016/j.margeo.2018.06.014

Maier, K. L., Rosenberger, K. J., Paull, C. K., Gwiazda, R., Gales, J., Lorenson, T., et al. (2019). Sediment and organic carbon transport and deposition driven by internal tides along Monterey Canyon, offshore California. *Deep Sea Research Part I: Oceanographic Research Papers*, *153*, 103108. https://doi.org/10.1016/j.dsr.2019.103108

McCann, M., Schramm, R., Cline, D., Michisaki, R., Harvey, J., & Ryan, J. (2014). Using STOQS (The Spatial Temporal Oceanographic Query System) to manage, visualize, and understand AUV, glider, and mooring data. *2014 IEEE/OES Autonomous Underwater Vehicles (AUV)*, 1–10. https://doi.org/10.1109/AUV.2014.7054414

Mitchell, N. C. (2014). Bedrock erosion by sedimentary flows in submarine canyons. *Geosphere*, *10*(5), 892–904. https://doi.org/10.1130/GES01008.1

Mountjoy, J. J., Howarth, J. D., Orpin, A. R., Barnes, P. M., Bowden, D. A., Rowden, A. A., et al. (2018). Earthquakes drive large-scale submarine canyon development and sediment supply to deep-ocean basins. *Science Advances*, *4*(3), eaar3748. https://doi.org/10.1126/sciadv.aar3748

Palanques, A., Durrieu de Madron, X., Puig, P., Fabres, J., Guillén, J., Calafat, A., et al. (2006). Suspended sediment fluxes and transport processes in the Gulf of Lions submarine canyons. The role of storms and dense water cascading. *Marine Geology*, *234*(1), 43–61. https://doi.org/10.1016/j.margeo.2006.09.002

Parsons, J. D., Bush, J. W. M., & Syvitski, J. P. M. (2001). Hyperpycnal plume formation from riverine outflows with small sediment concentrations. *Sedimentology*, *48*(2), 465–478. https://doi.org/10.1046/j.1365-3091.2001.00384.x

Parsons, J. D., Friedrichs, C. T., Traykovski, P. A., Mohrig, D., Imran, J., Syvitski, J. P. M., et al. (2007). The mechanics of marine sediment gravity flows. In C. A. Nittrouer, J. A. Austin, M. E. Field, J. H. Kravitz, J. P. M. Syvitski, & P. L. Wiberg (Eds.), *Continental margin sedimentation* (pp. 275–337). Blackwell Publishing Ltd. https://doi.org/10.1002/9781444304398.ch6

Paull, C. K., Caress, D. W., Ussler, W., III., Lundsten, E., & Meiner-Johnson, M. (2011). High-resolution bathymetry of the axial channels within Monterey and Soquel submarine canyons, offshore central California. *Geosphere*, *7*(5), 1077–1101. https://doi.org/10.1130/GES00636.1

Paull, C. K., Talling, P. J., Maier, K. L., Parsons, D., Xu, J., Caress, D. W., et al. (2018). Powerful turbidity currents driven by dense basal layers. *Nature Communications*, *9*(1), 4114. https://doi.org/10.1038/s41467-018-06254-6

Paull, C. K., Ussler, W., Greene, H. G., Keaten, R., Mitts, P., & Barry, J. (2002). Caught in the act: The 20 December 2001 gravity flow event in Monterey Canyon. *Geo-Marine Letters*, *22*(4), 227–232. https://doi.org/10.1007/s00367-003-0117-2

Paull, C. K., Ussler, W., III., Caress, D. W., Lundsten, E., Covault, J. A., Maier, K. L., et al. (2010). Origins of large crescent-shaped bedforms within the axial channel of Monterey Canyon, offshore California. *Geosphere*, *6*(6), 755–774. https://doi.org/10.1130/GES00527.1

Piper, D. J. W., & Aksu, A. E. (1987). The source and origin of the 1929 grand banks turbidity current inferred from sediment budgets. *Geo-Marine Letters*, *7*(4), 177–182. https://doi.org/10.1007/BF02242769

Postma, G., Cartigny, M., & Kleverlaan, K. (2009). Structureless, coarse-tail graded Bouma Ta formed by internal hydraulic jump of the turbidity current? *Sedimentary Geology*, *219*(1), 1–6. https://doi.org/10.1016/j.sedgeo.2009.05.018

Shepard, F. P. (1981). Submarine Canyons: Multiple causes and long-time persistence. *AAPG Bulletin*, *65*(6), 1602–1077. https://doi.org/10.1306/03B59459-16D1-11D7-8645000102C1865D

Slootman, A., & Cartigny, M. J. B. (2020). Cyclic steps: Review and aggradation-based classification. *Earth-Science Reviews*, *201*, 102949. https://doi.org/10.1016/j.earscirev.2019.102949

Smith, D. P., Kvitek, R., Iampietro, P. J., & Wong, K. (2007). Twenty-nine months of geomorphic change in upper Monterey Canyon (2002–2005). *Marine Geology*, *236*(1), 79–94. https://doi.org/10.1016/j.margeo.2006.09.024

Smith, D. P., Ruiz, G., Kvitek, R., & Iampietro, P. J. (2005). Semiannual patterns of erosion and deposition in upper Monterey Canyon from serial multibeam bathymetry. *GSA Bulletin*, *117*(9–10), 1123–1133. https://doi.org/10.1130/B25510.1

Sumner, E. J., Peakall, J., Parsons, D. R., Wynn, R. B., Darby, S. E., Dorrell, R. M., et al. (2013). First direct measurements of hydraulic jumps in an active submarine density current. *Geophysical Research Letters*, *40*(22), 5904–5908. https://doi.org/10.1002/2013GL057862

Talling, P. J. (2014). On the triggers, resulting flow types and frequencies of subaqueous sediment density flows in different settings. *Marine Geology*, *352*, 155–182. https://doi.org/10.1016/j.margeo.2014.02.006

Talling, P. J., Wynn, R. B., Masson, D. G., Frenz, M., Cronin, B. T., Schiebel, R., et al. (2007). Onset of submarine debris flow deposition far from original giant landslide. *Nature*, *450*(7169), 541–544. https://doi.org/10.1038/nature06313

Wang, Z., Xu, J., Talling, P. J., Cartigny, M. J. B., Simmons, S. M., Gwiazda, R., et al. (2020). Direct evidence of a high-concentration basal layer in a submarine turbidity current. *Deep Sea Research Part I: Oceanographic Research Papers*, 103300. https://doi.org/10.1016/j.dsr.2020.103300

Weimer, P., & Link, M. H. (1991). Global petroleum occurrences in submarine fans and turbidite systems. In P. Weimer & H. M. Link (Eds.), *Seismic facies and sedimentary processes of submarine fans and turbidite systems*. Springer. https://doi.org/10.1007/978-1-4684-8276-8_2

Winterwerp, J. C., Bakker Willem, T., Mastbergen Dick, R., & van Rossum, H. (1992). Hyperconcentrated sand-water mixture flows over erodible bed. *Journal of Hydraulic Engineering*, *118*(11), 1508–1525. https://ascelibrary.org/doi/10.1061/%28ASCE%290733-9429%281992%29118%3A11%281508%29

Xu, J. P. (2010). Normalized velocity profiles of field-measured turbidity currents. *Geology*, *38*(6), 563–566. https://doi.org/10.1130/G30582.1

Xu, J. P., Noble, M. A., & Rosenfeld, L. K. (2004). In-situ measurements of velocity structure within turbidity currents. *Geophysical Research Letters*, *31*(9). https://doi.org/10.1029/2004GL019718

Xu, J. P., Wong, F. L., Kvitek, R., Smith, D. P., & Paull, C. K. (2008). Sandwave migration in Monterey Submarine canyon, central California. *Marine Geology*, *248*(3), 193–212. https://doi.org/10.1016/j.margeo.2007.11.005

Zhang, Y., Liu, Z., Zhao, Y., Colin, C., Zhang, X., Wang, M., et al. (2018). Long-term in situ observations on typhoon-triggered turbidity currents in the deep sea. *Geology*, *46*(8), 675–678. https://doi.org/10.1130/G45178.1

References From the Supporting Information

Goto, S., & Matsubayashi, O. (2009). Relations between the thermal properties and porosity of sediments in the eastern flank of the Juan de Fuca Ridge. *Earth Planets and Space*, *61*, 863–870. https://doi.org/10.1186/bf03353197

Thomson, J. (2010). Observations of thermal diffusivity and a relation to the porosity of tidal flat sediments. *Journal of Geophysical Research*, *115*, C05016. https://doi.org/10.1029/2009JC005968